NAVAL POSTGRADUATE SCHOOL
Monterey , California

THESIS

AN ANALYSIS OF HYDROGRAPHIC DATA
COLLECTED OFF POINT SUR, CALIFORNIA
IN JUNE 1990

by

Georgios Th. Tziagidis

September 1991

Thesis Advisor   Newell Garfield

Approved for public release; distribution is unlimited.

REPORT DOCUMENTATION PAGE

1a Report Security Classification Unclassified		1b Restrictive Markings			
2a Security Classification Authority		3 Distribution Availability of Report			
2b Declassification Downgrading Schedule		Approved for public release; distribution is unlimited.			
4 Performing Organization Report Number(s)		5 Monitoring Organization Report Number(s)			
6a Name of Performing Organization Naval Postgraduate School	6b Office Symbol (if applicable) OC	7a Name of Monitoring Organization Naval Postgraduate School			
6c Address (city, state, and ZIP code) Monterey, CA 93943-5000		7b Address (city, state, and ZIP code) Monterey, CA 93943-5000			
8a Name of Funding Sponsoring Organization	8b Office Symbol (if applicable)	9 Procurement Instrument Identification Number			
8c Address (city, state, and ZIP code)		10 Source of Funding Numbers			
		Program Element No	Project No	Task No	Work Unit Accession No

11 Title (include security classification) AN ANALYSIS OF HYDROGRAPHIC DATA COLLECTED OFF POINT SUR, CALIFORNIA IN JUNE 1990

12 Personal Author(s) Georgios Th. Tziagidis

13a Type of Report Master's Thesis	13b Time Covered From To	14 Date of Report (year, month, day) September 1991	15 Page Count 71

16 Supplementary Notation The views expressed in this thesis are those of the author and do not reflect the official policy or position of the Department of Defense or the U.S. Government.

17 Cosati Codes			18 Subject Terms (continue on reverse if necessary and identify by block number)
Field	Group	Subgroup	California Undercurrent, Current, June 1990

19 Abstract (continue on reverse if necessary and identify by block number)

The data collected in June 1990 from the R/V Point Sur are used to study the California Undercurrent and California Current in the area off Point Sur. The area of study is a coastal region starting 3 km off Point Sur and extending westward 102 km. At that distance the orientation of the line of the stations changes to southwest, extending to 228 km offshore. The cruise took place from 16-22 of June under upwelling favorable weather conditions.

The results of this study help illustrate the great variability of the currents in the area. In June 1990 the California Undercurrent exists, is strong (max speed 36 cm/sec), is confined to the first 65 km from the shore, and carries equatorial type waters northward in depths less than 650 dbars. The estimated transport is 2.9 Sv. The California Current is broad, slower than the Undercurrent (max speed 28 cm/sec), shallower and carries Subarctic North Pacific waters. The coastal upwelling looks strong starting from the depth of 100 dbars, and contributes to the inshore coastal jet which it is observed in the first 3 km from the shore and in the upper 20 dbars.

Unlike previous analyses based on CalCOFI data, the Undercurrent appears robust in June. Its strong surface and subsurface signature had not previously been reported for this month. This may in part be due to the determination made in this thesis that 700 dbar is a more appropriate reference level than either 500 or 1000 dbar.

20 Distribution Availability of Abstract			21 Abstract Security Classification		
☒ unclassified unlimited ☐ same as report ☐ DTIC users			Unclassified		
22a Name of Responsible Individual Newell Garfield			22b Telephone (include Area code) (408) 646-3226		22c Office Symbol OC/GF

DD FORM 1473,84 MAR 83 APR edition may be used until exhausted security classification of this page
All other editions are obsolete

i

An Analysis Of Hydrographic Data
Collected Off Point Sur, California
In June 1990

by

Georgios Th. Tziagidis
Lieutenant, Hellenic Navy
B.S., Hellenic Naval Academy

Submitted in partial fulfillment of the
requirements for the degree of

MASTER OF SCIENCE IN PHYSICAL OCEANOGRAPHY

from the

NAVAL POSTGRADUATE SCHOOL
September 1991

ABSTRACT

The data collected in June 1990 from the *R/V Point Sur* are used to study the California Undercurrent and California Current in the area off Point Sur. The area of study is a coastal region starting 3 km off Point Sur and extending westward 102 km. At that distance the orientation of the line of the stations changes to southwest, extending to 228 km offshore. The cruise took place from 16-22 of June under upwelling favorable weather conditions.

The results of this study help illustrate the great variability of the currents in the area. In June 1990 the California Undercurrent exists, is strong (max speed 36 cm/sec), is confined to the first 65 km from the shore, and carries equatorial type waters northward in depths less than 650 dbars. The estimated transport is 2.9 Sv. The California Current is broad, slower than the Undercurrent (max speed 28 cm/sec), shallower and carries Subarctic North Pacific waters. The coastal upwelling looks strong starting from the depth of 100 dbars, and contributes to the inshore coastal jet which it is observed in the first 8 km from the shore and in the upper 20 dbars.

Unlike previous analyses based on CalCOFI data, the Undercurrent appears robust in June. Its strong surface and subsurface signature had not previously been reported for this month. This may in part be due to the determination made in this thesis that 700 dbar is a more appropriate reference level than either 500 or 1000 dbar.

TABLE OF CONTENTS

LIST OF TABLES

LIST OF FIGURES

I. INTRODUCTION

A. GENERAL CLIMATOLOGICAL PICTURE

In 1987, the Point Sur Transect (POST) was established by the Department of Oceanography at the Naval Postgraduate School to investigate the long term variability in the eastern Pacific boundary region. Since its establishment 12 cruises were undertaken and seven theses have been accomplished using these data. This research, the 8th report, deals with the data from June 1990 for the investigation of California Undercurrent at Point Sur.

The following description is taken from Berryman (1989) to give the general climatological picture.

"The California Current (CC) is the eastern boundary current of the Subtropical North Pacific gyre, and extends from Washington State to Baja California. Typical of eastern boundary currents it is a broad, shallow and weak system of equatorial flow. Velocities are usually less than 25 cm/sec, most of the flow is limited to the top 300 m and the system extends from the coast out to 900 km with a core 200 - 300 km offshore. Low temperature, low salinity subarctic water originating near the West Wind Drift is carried south and mingles with the other water masses found in the region. These are the eastern North Pacific water mass on the western boundary of the California Current, and Equatorial Pacific water from the South.

"In addition to the broad equatorial flow, the system is characterized by a poleward under current closer inshore, variously called the inshore Countercurrent (IC), or the Davidson Inshore Current (DIC) when it reaches the surface. This poleward flow is somewhat stronger, more narrow, and generally found over the continental slope and shelf. While the equatorward flow of the California Current is fairly consistent year-round, the countercurrent exhibits strong annual variability, alternately kept at depth in the spring and summer as a result of the strong northwesterly winds, and surfacing in the fall and winter with the relaxation of the winds."

The annual picture of the nearshore water characteristics is constructed as follows. Cool, high salinity, high nutrient waters dominate the nearshore waters of the central coast from February to September. This is the upwelling period of strong northwesterly winds. In September the winds diminish resulting in the encroachment of the oceanic water into the nearshore areas; this is the oceanic period which usually persists until

November. As the winds shift to the southwest in November, the northward flowing Counter Current reaches to the surface landward of the California Current, and then is known as the Davidson Current. This northward surface flow of warm, low salinity water persists until the winds reverse in February.

B. STUDIES ON THE AREA

The California Current system has been the subject of numerous studies in the past, from the long-term data collection of California Cooperative Oceanic Fisheries Investigations (CalCOFI) to specific process experiments of recent years such as the Coastal Transition Zone Program (CTZ Program), Central California Coastal Circulation Study (CCCCS), and the Point Sur Transect (POST) (Berryman 1989, Tisch 1990).

The CalCOFI data set represents a forty year record of hydrographic surveys aimed at examining the long term variability of the coastal region and the enviromental impact on local fisheries. An excellent review of the CalCOFI program can be found in the October 1988 CalCOFI Reports (Reid 1988). Summary of the seasonal variability of the flow according to the CalCOFI data is given by Hickey (1979) and Chelton (1984). Velocities were derived from these hydrographic data using an assumed level of no motion (LNM) with the geostrophic relationship.

The CCCCS program (February 1984 to July 1984) provided higher hydrographic resolution (than CalCOFI) and included moored current meter arrays from San Francisco to Point Conception. The important conclusion drawn from this experiment was that the historical CalCOFI hydrographic data do not resolve spatial scales of variability in shelf and slope waters because the horizontal spacing of stations was too coarse to resolve the coastally trapped poleward flow (Chelton et al. 1987). The most notable feature thus identified in the CCCCS was the relatively consistent coastally trapped poleward flow over the shelf in the entire region from Point Conception to San Francisco. The cause of this mean poleward flow and the large fluctuations in the flow were not identified. These features appear to be unrelated to local wind forcing, which is generally equatorward in the region and varies on a much shorter time scale (Chelton et al. 1987).

In 1987 the Point Sur Transect (POST) was established by the Department of Oceanography at the Naval Postgraduate School (NPS) to investigate the long term variability in this region. Investigating the time variability of poleward flows, their role in gyre-scale processes, and related dynamics are the main goals. POST extends offshore, normal to bottom topography, along 36°N to 123°01.7 W. There it turns along the es-

2

tablished CalCOFI line 67 (the Monterey Bay line) to allow for comparison with previous studies utilizing the CalCOFI data set. As of June 1990 there had been 19 cruises (Table 1) along the POST (Figure 1).

Table 1.   POINT SUR TRANSECT CRUISE PERIODS AND DATA TYPE

Cruise	Dates	Vessel	Data type
STNOV 1987	11/4 - 11/11	R/V Point Sur	CTD.ADCP
CUC-April 1988	4/15 - 5/1	USNS DeSteiguer	CTD ADCP PEGASUS
STMAY 1988	5/4 - 5/11	R/V Point Sur	CTD ADCP
CUC-August 1988	8/3 - 8/7	R/V Point Sur	CTD ADCP PEGASUS
CUC-September 1988	9/22 - 9/27	R/V Point Sur	CTD ADCP PEGASUS
STNOV 1988	11/1 - 11/8	R/V Point Sur	CTD ADCP
CUC-November 1988	11/14 - 11/19	R/V Point Sur	CTD ADCP PEGASUS
CUC-February 1989	2/3 - 2/7	R/V Point Sur	CTD ADCP PEGASUS
CUC-March 1989	3/24 - 3/30	R/V Point Sur	CTD ADCP PEGASUS
CUC May 1989	5/10 - 5/26	USNS DeSteiger	CTD ADCP PEGASUS
STMAY 1989	5/4 - 5/26	R/V Point Sur	CTD ADCP
CUC-July 1989	7/28 - 8/3	R/V Point Sur	CTD ADCP PEGASUS
CUC-September 1989	9/25 - 9/30	R/V Point Sur	CTD ADCP PEGASUS
STNOV 1989	11/1 - 11/8	R/V Point Sur	CTD ADCP
CUC-November 1989	11/15 - 11/22	R/V Point Sur	CTD ADCP PEGASUS
CUC-January 1990	1/17 - 1/24	R/V Point Sur	CTD ADCP PEGASUS
CUC-March 1990	3/19 - 3/26	R/V Point Sur	CTD ADCP PEGASUS
STMAY 1990	5/2 - 5/8	R/V Point Sur	CTD ADCP
CUC-May 1990	5/17 - 5/23	R/V Point Sur	CTD ADCP PEGASUS
CUC-June 1990	5/16 - 5/22	R/V Point Sur	CTD ADCP PEGASUS

Figure 1 gives the distribution of the stations on the Point Sur Transection used for the California Undercurrent (CUC) project. This thesis deals with the CUC, using the data from the June 1990 cruise, and consists of 22 CTD stations and 9 Pegasus stations. The length of the hydrographic transection is 228 km with denser coverage at the inshore end of the transection.
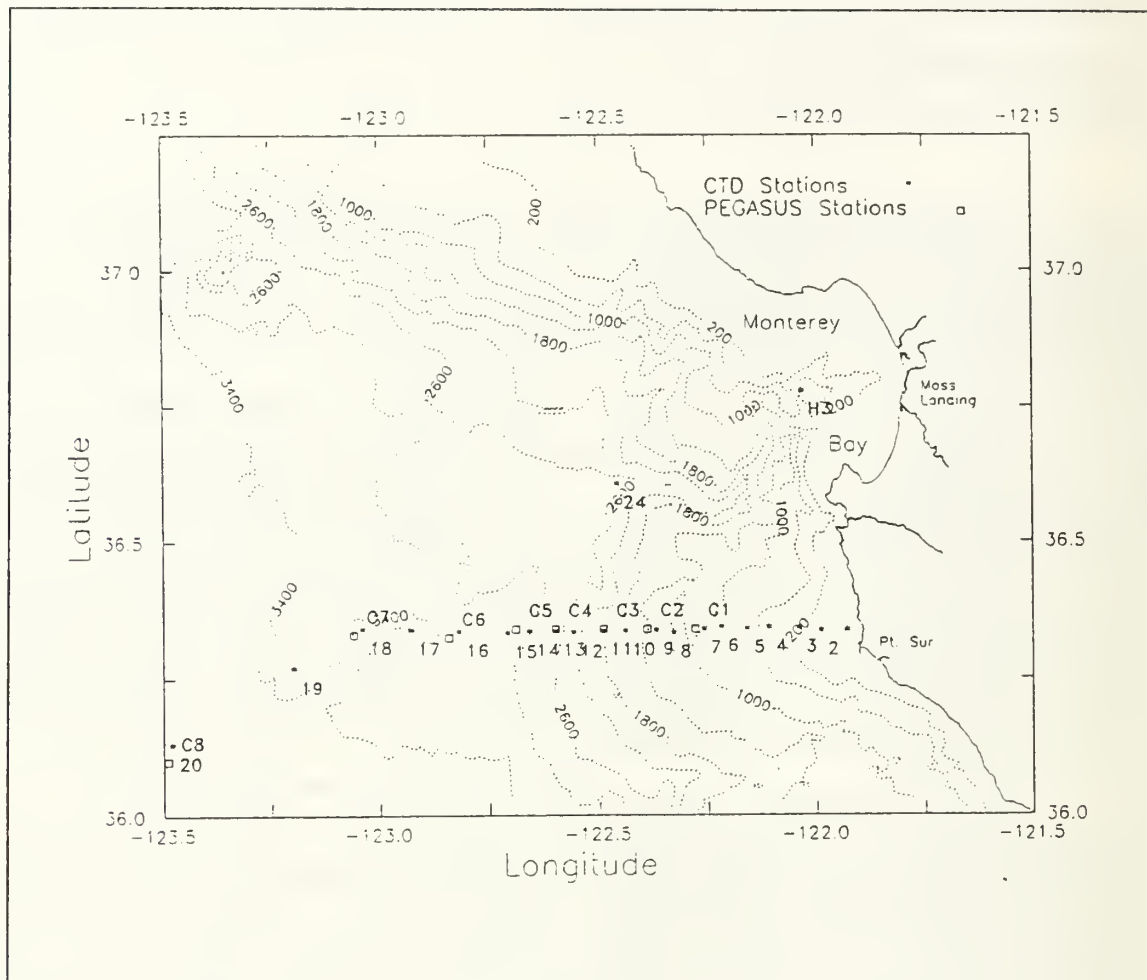
Figure 1.   The scheme of the POST

This study of the CUC also utilizes continuous vertical profiles of absolute velocity from the "Pegasus" instrument. This instrument allows accurate velocity data to be collected rapidly and with greater ease over a large geographic region, and removes the guesswork associated with erroneous assumptions about levels of "No Motion" (Berryman 1989). The difficulty with using instruments like "Pegasus" is in separating the velocity constituents since it is an instantaneous measurement. Bimonthly sampling prevents temporal resolution of less than four months.

Previous studies of the area by the NPS students showed that a narrow poleward undercurrent exists close to the shore. The speed and the location vary from season to season. The nature of the alongshore geostrophic velocities and the location and spatial

4

extent of the Undercurrent appear to be strongly related to specific wind events, local and remote (Tisch 1990). Table 2 (from Tisch 1990) shows the spatial extent and core velocities of the California Undercurrent based upon the geostrophic relationship relative to 1000 dbars for data from the seven selected cruises.

Table 2. SPATIAL EXTENT OF THE UNDERCURRENT BASED ON PREVIOUS STUDIES (Tisch, 1990)

Cruise	Core distance from the shore (Km)	Core depth (m)	Maximum Velocity (cm/sec)
STMAY 1988	22	460	< 5
CUC-August 1988	12 / 42	190	> 35 / > 20
CUC-November 1988	20	460	> 25
CUC-February 1989	15	100	> 35
STMAY 1989	17	160	> 20
CUC-July 1989	23	400	> 10
CUC-November 1989	28	70	> 35

C. POINT SUR

1. Geophysical characteristics

The continental margin off Point Sur consists of a shelf extending some 15 km from the coast to a depth of 150 m, a steeper continental slope out 75 km to a depth of 3050 m, and a gentler rise to the basin floor 3500 m deep, about 100 km offshore. A ridge starting at Point Sur and extending offshore (west) a distance of about 34 km may affect the currents in the area.

Numerous canyons indenting the shelf (Figure 2) may affect the currents in the area. Sur Canyon, located off the Big Sur River, heads 5.5 km from land near one of the local rivers. However, an intersecting canyon, Partington Canyon, extends almost to the beach. Partington's Canyon head bends along the coast.

The Sur-Partington group has five main branches. The channels are twisting like the pattern of a river. The canyons are V-shaped, but are flattened at a depth 620 m. The Sur canyon branch is cut deepest into the slope with walls as high as 620 m in some places. The whole canyon system (Sur and Partington) extends offshore for 89 km from the head of the Sur canyon, or 107.5 km from the head of Partington canyon.
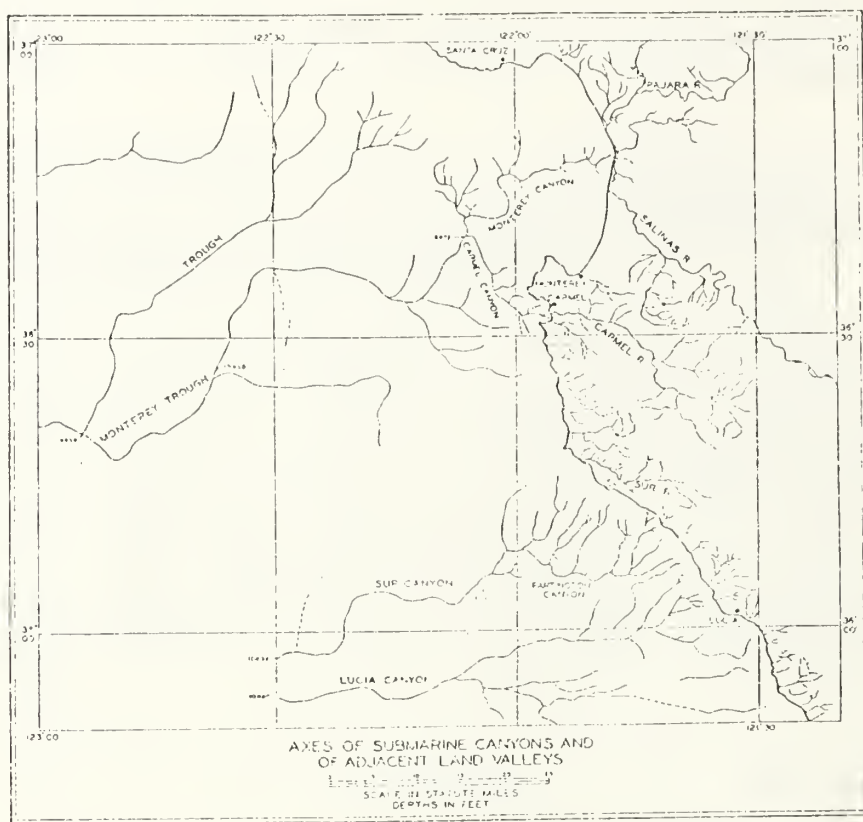
Figure 2. Geophysical characteristics of the area - Canyons (Shepard 1941)

The largest submarine canyon along the California coast is the Monterey Submarine Canyon. It heads in Monterey Bay (Moss Landing and Moss Lagoon) and extends seaward at a distance 195 km. Carmel Submarine Canyon heads on Carmel Bay and extends seaward first west then northwest coming into Monterey Submarine Canyon at a depth 2000 m. Transverse profiles of both Monterey Canyon and Carmel Canyon, indicate that a V-shape predominates in the inner portions of the canyons. Further out where the trend of Monterey Canyon changes direction from west to southwest, it loses its V-shape and becomes a broad trough without particularly high or steep walls. These two canyons may play an important role in the currents in the area.

2. Water masses

To study the water types at Point Sur, first we have to see what are the characteristic water masses in North Pacific which contribute in the formation of the water masses at Point Sur. The North Pacific water masses according to Defant (1941) are given in Table 3. The limiting values for temperature and salinity are given to demonstrate in what extreme limits oceanographic factors may vary.

Table 3. WATER MASSES OF NORTH PACIFIC ACCORDING TO DEFANT (1941)

NorthPacific	Temperature (°C)	Salinity (psu)
Subarctic Water	2-10	33.5-34.4
Pacific Equatorial Water	6-16	34.5-35.2
Eastern North Pacific Water	10-16	34.0-34.6
Western North Pacific Water	7-16	34.1-34.6
Arctic Intermediate Water	6-10	34.0-34.1
Pacific Deep Water and Arctic Circumpolar Water·	(-1)-3	34.6-34.7

Tchernia (1980) gives a simple picture of the water masses in North Pacific, but as Defant, he puts limiting values of temperature and salinity (Table 4).

Table 4. WATER MASSES OF NORTH PACIFIC ACCORDING TO P. TCHERNIA (1980)

NorthPacific	Temperature (°C)	Salinity (psu)
Subarctic Water	5	33
North Central Pacific water	12	35
Arctic intermediate water	5	34

Sverdrup, Johnson, and Fleming (1961) give the water masses in the area in a more moderate way, avoiding temperature and salinity limits. According to them, the water mass which dominates in all the North Pacific is the Subarctic Water mass. At 50 °N this water mass is characterized by an average temperature between 2 and 4 °C and salinity 32 psu but increases to approximately 34 psu at a depth of a few hundred meters and below that depth increases slowly to about 34.65 psu at the bottom. This water mass

is carried toward the east and when reaching the American coast it is deflected toward the south and enters to a region of different climatic conditions. Here the temperature of the upper layers is raised by heating and the salinity is increased by excess evaporation and mixing, so that the T,S curves gradually swing toward the right. Strictly speaking, the Subarctic Water mass is characterized as the water mass northward of 45° N. For the sake of convenience this name is used for all the water mass until of 23° N. Southward from this latitude the Subarctic Water mass converges with the Equatorial Water mass. Between 22° N and 45° N and below 300 m the T-S curves show waters intermediate in character between Subarctic North Pacific and the Equatorial Water. This fact suggests that the water at this area is formed by lateral mixing between those two large and well defined water masses. Such mixing gives the idea that a northward penetration of Equatorial water occurs along the coast. Sverdrup and Flemming (1941) and Tibby (1941) observed that at stations close to the shore (30 km from the shore) the water mass had characteristics closer to Equatorial Water mass than to Subarctic Water mass. For the same latitude, water mass at a station 550 km from the shore had characteristics closer to Subarctic Water mass. From the above description it is evident that close to the shore we expect the Subarctic North Pacific water mass to be strongly affected by the Equatorial Water mass characteristics. Offshore the waters are expected to be more likely to be Subarctic North Pacific water mass.

The following currents and phenomena are the main contributors in formation of the water masses at Point Sur. .

- The warm and salty northward flowing California Undercurrent close to the shore
- The cold and low salinity southward flowing California Current offshore.
- The strong upwelling, during the spring and summer which mixes subsurface water with surface water masses.
- The coastal jet (5 to 25 km offshore) and
- The Davidson Current, which brings oceanic surface water close to the shore.

The California Undercurrent and its T-S relationship are discussed by Sverdrup and Fleming (1941), Tibby (1941), Blanton and Pattullo (1970), Reid Roden and Wyllie (1958), Halpern Smith and Reed (1978), Wooster and Jones (1970), Wickham (1975) and Chelton (1984), who may be the most representative author for the area Off Point Sur. The results from the above works, except Chelton's, are summarized in Hickey (1979). According to these authors the California Undercurrent flows over the continental slope and carries equatorial type water. This water is characterized by high temperature,

8

salinity and phosphate, and low dissolved oxygen. From dynamic topography of the 200 dbar surface, Reid (1958) showed that at depths greater than 200 dbars there is poleward flow throughout most of the year from southern Baja to at least as far north as Cape Mendocino in northern California.

The current meter records of Collins et al. (1968) and Mooers et al. (1976) suggest that the undercurrent over the shelf is highly coupled to the equatorward wind stress. According to these, strong upwelling favorable winds result in an equatorward surface jet and poleward undercurrent.

Hickey (1979) concludes that the salinity and temperature of the core of California Undercurrent in all the range from Baja California to Vancouver Island is between 34.6 psu and 9.5 $^{\circ}C$ (observed at Baja California) and 33.9 psu and 7.0 $^{\circ}C$ (observed at Vancouver Island). Mixing processes diminish the cross-shore temperature and salinity gradients so the transition observed in the waters off Vancouver Island is much more gradual than off southern California. The seasonal variation of the percentage of Equatorial water at specific locations along the coast has not been investigated. Wooster and Jones (1970) believe and give some evidence for interannual variations in northward extent of a given isohaline.

The most representative author for the area off Point Sur is Chelton (1984). Using geostrophy he found that the California Undercurrent at Point Sur presents variations year-round. During June, he found no evidence for an undercurrent. It was never observed during the June and only weak poleward flow has ever been observed in July.

According to Hickey (1979): "The California Current exists in two regions of southward flow. The nearshore region is most fully developed in spring and early summer south of Cape Blanco. The offshore region is most fully developed in late summer or fall. Of the two southward regions the nearshore region is strong year-round. This region moves closer to the shore towards the south from Cape Medocino and carries low salinity cold water. Pavlova (1966) found that the maximum southward flow occurs at the surface in all the seasons, at about 300-500 km offshore of Point Conception and agrees with Wyllie's (1966) data in the offshore region. The California Current is more fully developed in the area during the spring and early summer. This agrees with conclusions based on Wyllie's data only if the region sampled corresponds with the nearshore branch of the current". Refering to Chelton (1984) for the California Current off Point Sur: "The core of California Current is located between 100 and 200 km offshore and is mostly restricted to the upper 200 m. The seasonal variability of this core shows two equatoward maxima per year with peak velocity of 9 cm/sec in February-

March and again July-August. The core is displaced slightly farther offshore in the wintertime maximum."

The coastal jet is mentioned in all the descriptions of shelf circulation along the coast of California and occurs during the upwelling season. This is a southward flow very close to the shore with a maximum speed at a distance 5 to 25 km from the coast. It is strongest during the spring and is centered closer to the shore than during the summer. The transported waters are mainly upwelled waters rich in phytoplankton and oxygen. Chelton (1984) describes that during March-April and July-September there is a narrow second maximum equatorward flow very nearshore with velocities of 5 to 8 cm/sec. He supposes that this jet may be more intense over the continental shelf, but with the CalCOFI data he couldn't support this hypothesis.

Poleward surface flow in nearshore regions off the coast of California associated with winter weather patterns is known as the Davidson Current. The Davidson Current is developed near the coast north of Point Conception in fall and winter and causes dramatic changes in water properties south of Cape Medocino. It brings southern oceanic water northward and reinforces the idea that the Davidson Current is the surface expression of the California Undercurrent which carries Equatorial type water northward.

3. Weather conditions

Weather conditions during the cruise are given in Figure 3. As it can be seen the wind during all the cruise was from NW directions as usually happens in this season in the area (Huyer 1983). The wind speed was ranged from 6 to 12 m/sec contributing in the process of the upwelling in area. Air temperature was relatively high, staying above 12° C.

4. Purpose of the study - Contents

The data were collected during 16 - 21 June 1990 aboard the *RV Point Sur*. The purpose of this study is to analyse and interpret these data, comparing the results to the previous conclusions. In particular, I describe the spatial structure of the various currents, flows or jets, and compare geostrophic flow with absolute current measurements.

In this report Chapter II covers the instruments, methods, and data processing techniques. Chapter III provides detailed analyses of the results. Finally Chapter IV summarizes the conclusions and offers recommendations for future work.
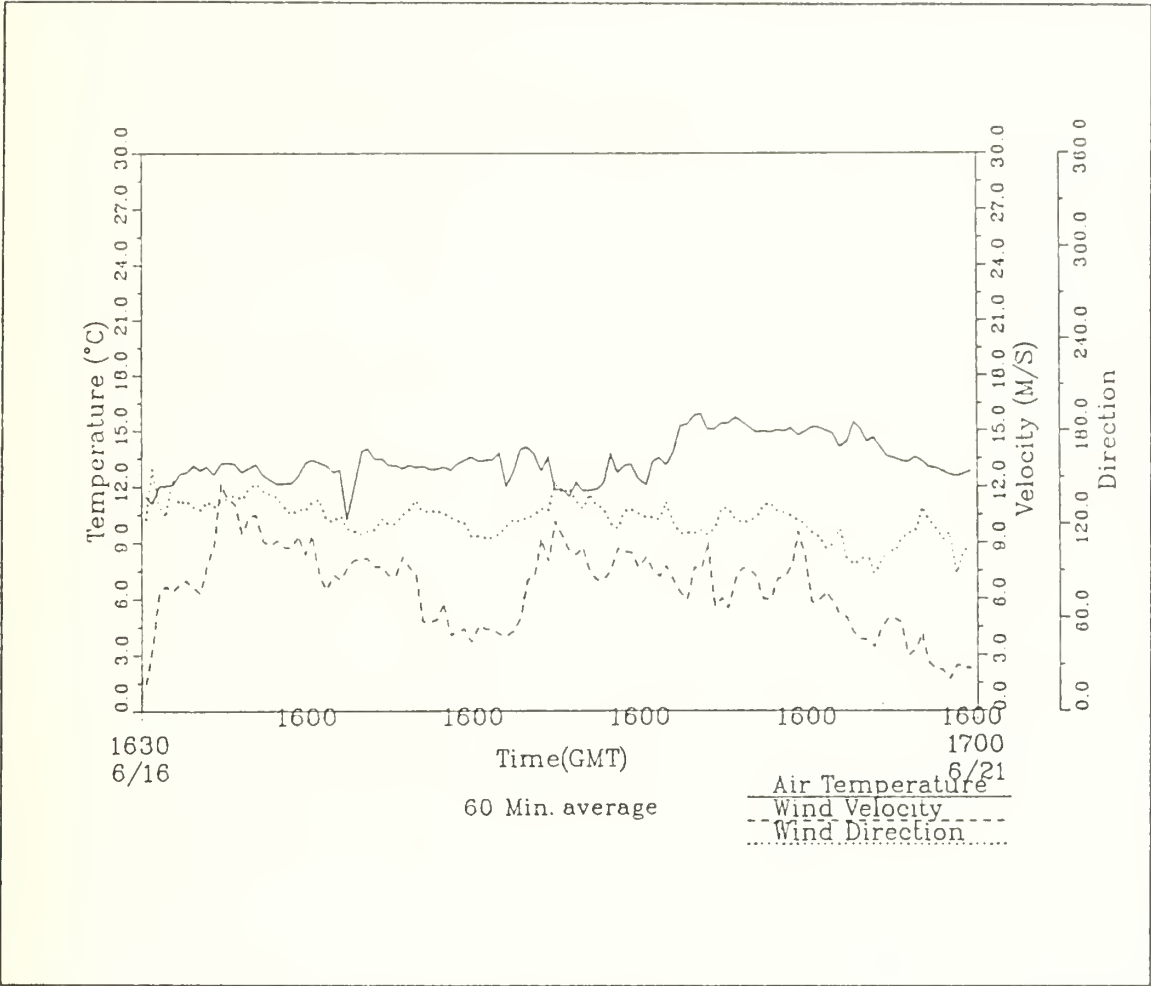
Figure 3.   Weather conditions during the cruise

11

II. DATA COLLECTION AND PROCESSING

The Pt Sur data transection (Figure 1) of 22 CTD stations and 9 Pegasus sites is designed to resolve the water mass structure in the slope region.

A. DATA COLLECTION

1. Pegasus

The Pegasus instrument is an acoustically tracked dropsonde which free falls through the water column and returns to the surface after dropping weights at the bottom. The elapsed times from the broadcast of a 10 KHz signal sent by Pegasus and the response by each of at least two bottom-mounted (and surveyed) transponders are recorded internally. Travel times are later converted to distances using a sound speed profile. The location of Pegasus as it falls through the water column is determined based on the consecutive ranges relative to the transponders and the depth. Velocities are derived from this path by differentiation with respect to time. The instrument transmits once every 16 seconds and with nominal fall and ascent rates of 30 - 35 m/min, data are recorded at about 8 m increments. The horizontal speeds are accurate to within 1 - 3 cm/sec, with uncertainties arising from assumptions regarding the speed and path of sound through the water column, as well as signal deformation and detection (Berryman 1989).

Pegasus cast locations begin 33 km from the coast. The first 7 sites are spaced 10 km apart along latitude 36°20 N (Figure 1). Sites 8 and 9 are located on CalCOFI line 67, 50 km and 123 km, respectively from site 7. Table 5 lists the pertinent Pegasus site information.

Each cast extends from the surface to the bottom. In order to facilitate the elimination of inertial oscillations (at this latitude the inertial period is about 20 hours), the stations were surveyed twice, with approximatelly 9 to 11 hours between casts. Each cast has two independent profiles (upward and downward) which can be analyzed separately or combined into an average profile. Totally 36 profiles were collected by Pegasus during the cruise of June 90 and 34 were analyzed. Cast # 267 have not taken into account because the data were insufficient.

2. ADCP

The RD Instruments Inc. Acoustic Doppler Current Profiler (ADCP) is a vessel-mounted instrument (Model VM-ADCP) which utilizes the range-gated Doppler

Table 5.   PEGASUS SURVEY

Cast, Sta# Distance from the shore (km)	Date, Time (Z)	Location	Depth (dbars)
258, C1/32.8	6, 17 03:36	36°20.12N 122°16.22W	1022
259, C2/43.4	6, 17 07:48	36°20.31N 122°23.17W	1380
260 C1/32.8	6/17 14:00	36°20.12N 122°16.30W	1023
261 C2/43.4	6, 17 16:12	36°20.35N 122°23.03W	1343
262, C3/54.1	6, 17 15:55	36°20.27N 122°29.25W	1909
263 C4/63.1	6 18 01:55	36°20.06N 122°35.65W	2618
264 C3/54.1	6, 18 06:12	36°20.38N 122°29.22W	1883
265/C4/63.1	6/18 12:27	36°20.05N 122°35.73W	2620
266 C5/71.9	6 18 16:00	36°19.05N 122°41.04W	3184
267, C5/71.9	6/19 02:23	36°18.97N 122°41.10W	3189
268 C6 82.7	6 19 07:10	36°19.30N 122°50.70W	3161
269, C7/102.1	6 19 12:28	36°19.49N 123°02.86W	3611
270 C6/82.7	6, 19 17:40	36°19.42N 122°50.56W	3139
271 C7/102.1	6/19 22:28	36°19.29N 123°02.88W	3591
272 C8/144.7	6 20 05:32	36°05.86N 123°28.85W	3624
273/C8/144.7	6/20 18:21	36°05.79N 123°28.77W	3623
274 C9/212.7	6 21 02:46	35°46.22N 124°12.46W	4012
275/C9/212.7	6 21 12:13	35°46.25N 124°12.44W	4013

shift of the signal backscattered from water particles along four column. The relative velocities are made through accurate knowledge of the ship's motion. Details of the ADCP can be found in Kosro (1985), RD Instruments (1989), and Moschovos (1989).

The accuracy of the ADCP is highly dependent on the quality of the ship's navigational data used to convert the relative velocities measured by the ADCP into absolute velocities. Variability of the ship's speed and direction and data collection interval play significant roles in the ADCP accuracy and reliability. If these parameters are not carefully integrated it will lead to considerable uncertainty in the final velocities. Kosro (1985) and King (1989) state accuracies of 4-5 cm/sec in the U component and 2-4 cm/sec in the V component relative to current meters.

3.   CTD

Casts were made at 22 stations utilizing a MK III Neil Brown CTD probe with manufacturer sensitivities listed in Table 6.

Table 6.   MK III NEIL BROWN PROBE (MANUFACTURER'S SENSITIV-ITIES)

Variable	Range	Accuracy	Resolution
Pressure	0-3200 db	+ 3.2 db	0.05 db
Temperature	-3 to +32"C	+ 0.005^0	0.0005^{0}C
Conductivity	1 to 65 mmho	+ 0.005 mmho	0.001 mmho

Water samples were taken at the bottom, 3000 m and 1000 m of each cast from which salinity values were then determined in the laboratory. The raw CTD data were calibrated using the bottle samples. Figure 4 shows the residual difference after calibration which has a standard deviation of 0.005. Table 7 gives details of the CTD survey.

B.   DATA PROCESSING

1.   Pegasus

The initial data processing was done by Tarry Rago using programs written at the University of Rhode Island and modified for use at the Naval Postgraduate School. Travel times were hand-edited and converted to velocities to remove obviously bad points, and then vertically smoothed using a 30 meter Hamming halfwidth filter. This resulted in four independent profiles for each Pegasus station, which could then be averaged together to obtain an average velocity profile at the station with inertial effects partially removed. The result of the above mentioned calibration was 34 profiles which were used for the analysis. Two profiles of the cast 267 were rejected because insufficient good data were recorded.

2.   ADCP

Briefly stated, the first step in processing the ADCP raw data is the calculation of ship's velocity from the navigation data. From this navigation data the U and V components of ship's velocity are calculated.

The next step in processing is the initial determination of the depth to which the data of each ensemble remains reliable. The basic criterion for this step comes from the good percent of return echoes (BIN STATISTICS FILE). By subtracting the ship's velocity from the average velocity within the chosen reference layer, an absolute reference
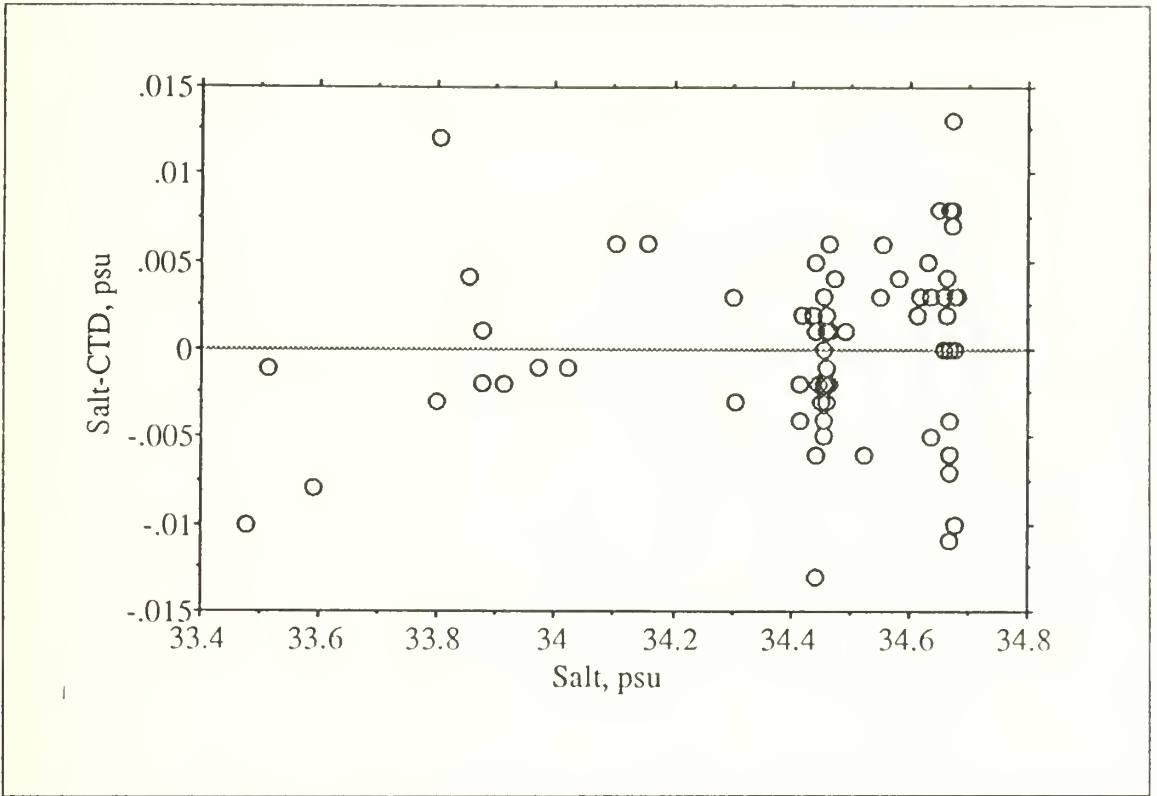
Figure 4.   Difference between CTD salinity and laboratory determined salinity over the sampled range

layer velocity for each ensemble is obtained. The series of absolute reference velocities is then filtered with low pass Hamming window filter.

Once the absolute reference velocity is determined, the velocity profiles of each ensemble with respect to their reference velocity are also determined, thus yielding the final profiles of absolute water velocity. The profiles of absolute velocity are then averaged over the time interval for each run. Detailed description of converting the relative velocities into absolute velocities is contained in theses of Reece (1989) and King (1989).

The ADCP data were initially processed by Tarry Rago using programs written by Paul Jessen of the Naval Postgraduate School's Oceanography Department. The processed profiles were averaged over 30 minutes in time and filtered vertically using a Hamming window with a 2 bin halfwidth. The reference layer chosen was 28-48 m, based on a "good ping" return of at least 95 percent in that layer.

Table 7. CTD SURVEY

Cast # / Distance from the shore	Date/Time (Z)	Location	Depth
1/3.62	6/16 2137	36°20.06N 121°56.24W	47
2/8.10	6/16 2232	36°20.07N 121°59.17W	100
3/12.28	6/16 2302	36°20.13N 122°01.96W	128
4/17.21	6/16 2334	36°20.14N 122°05.27W	301
5/22.58	6/17 0043	36°20.15N 122°08.85W	673
6/28.70	6/17 0138	36°20.04N 122°13.01W	934
7/32.13	6/17 0228	36°20.07N 122°15.34W	988
8/37.96	6/17 0540	36°19.94N 122°19.15W	966
9/42.29	6/17 0642	36°20.05N 122°22.14W	1202
10/47.66	6/17 0957	36°20.08N 122°25.72W	1652
11/52.14	6/17 1130	36°20.09N 122°28.68W	1851
12/58.56	6/17 2157	36°19.98N 122°33.00W	2202
13/62.29	6/17 2354	36°19.96N 122°35.47W	2615
14 67.82	6/18 0946	36°20.06N 122°39.21W	3131
15/72.59	6/18 1619	36°20.26N 122°42.38W	3170
16/81.25	6/18 2046	36°20.00N 122°48.17W	3032
17/88.42	6/18 2308	36°19.98N 122°52.97W	3250
18/102.15	6/19 1245	36°19.96N 123°02.20W	3569
19 118.52	6/19 2328	36°15.61N 123°11.65W	3346
20/150.35	6/20 0540	36°06.70N 123°29.88W	3610
21 188.07	6/20 1143	35°56.76N 123°51.90W	3930
22 228.17	6/21 0312	35°45.39N 124°14.58W	3842

3.   CTD

Initial processing of the CTD data was conducted using programs written by Jim Stockel. The data were edited for bad points and averaged into 2 meter bins. After precruise laboratory temperature and conductivity calibration, an error still existed between bottle salinity values and "calibrated" salinity values in the CTD data file. To correct this error, conductivity measurements were calibrated to water samples and the CTD data were further adjusted using the polynomial least squares regression fit men-

tioned before. Density, dynamic height, and geostrophic velocities were calculated from the calibrated CTD data using Paul Jessen's programs based on the equation of state, EOS 80, (Fofonoff, 1985) and "dynamic method" as described by Fomin (1964).

III. ANALYSIS

A. DESCRIPTION

1. Hydrography

This section first presents detailed descriptions of the temperature, salinity, and density fields. The results from these enable us to proceed further in the analysis of T/S characteristics, spiciness and to distinguish the water masses in the area. I then try to approximate the level of no motion (LNM) using Defant's method (1941). From the resulting LNM I create the dynamic topography and geostrophic velocity cross-sections. The results from these are compared with the results taken using LNM 500 and 1000 dbars.

2. Temperature

Temperature profiles of the stations can be described better if they are first divided in three distinct zones as follows:

- "Surface zone". This zone starts from the surface and extends downward to 100 dbars. This is the zone which is affected strongly from the atmosphere so the changes in temperature are abrupt and distinct. One important characteristic in this layer is the variation of the mixed layer depth (MLD). Starting from the shore (Figure 6) the MLD is very shallow and lies between 10 to 30 dbars. As the distance increases the MLD increases too, reaching 80 dbars at stations far offshore. From Station 1 to Station 18 strong spatial changes of temperature occur, giving an idea that different water masses are in the area. At Station 1 the water temperature is the lowest, from Station 1 to Station 5 (22 Km offshore) increases, further offshore to Station 9 (42.4 Km offshore) decreases. Stations 9 and 10 mark the boundary of two different water masses. From Station 10 to Station 13 an increase of the water's temperature is shown and further offshore to Station 16 a decrease. The picture becomes more clear offshore from Station 16 where continuous increase of the water's temperature is shown.

  Another interesting feature in this zone is the upward slope toward the east of the isotherms in almost the entire range from shore to Station 18. This will be discussed later in detail.

- "Second zone or Thermocline". I name "Thermocline" the zone from 100 to 1000 dbars to include all that happens in the layers where the temperature decreases (first rapidly and then slowly) until the water gets its permanent temperature at depth. Comparing the temperature profile of all the stations in this zone with that in the previous described zone, we see that temperature reveals the same trend in variability as in the previous with smaller magnitude. The upward bend of the isotherms close to the shore continues until the depth of 130 dbars and becomes steepest inshore. Below 130 dbars the isotherms bend downward and this happens until the depth of 600 dbars.

  Connecting these observations with those in the previous zone, we can say that:
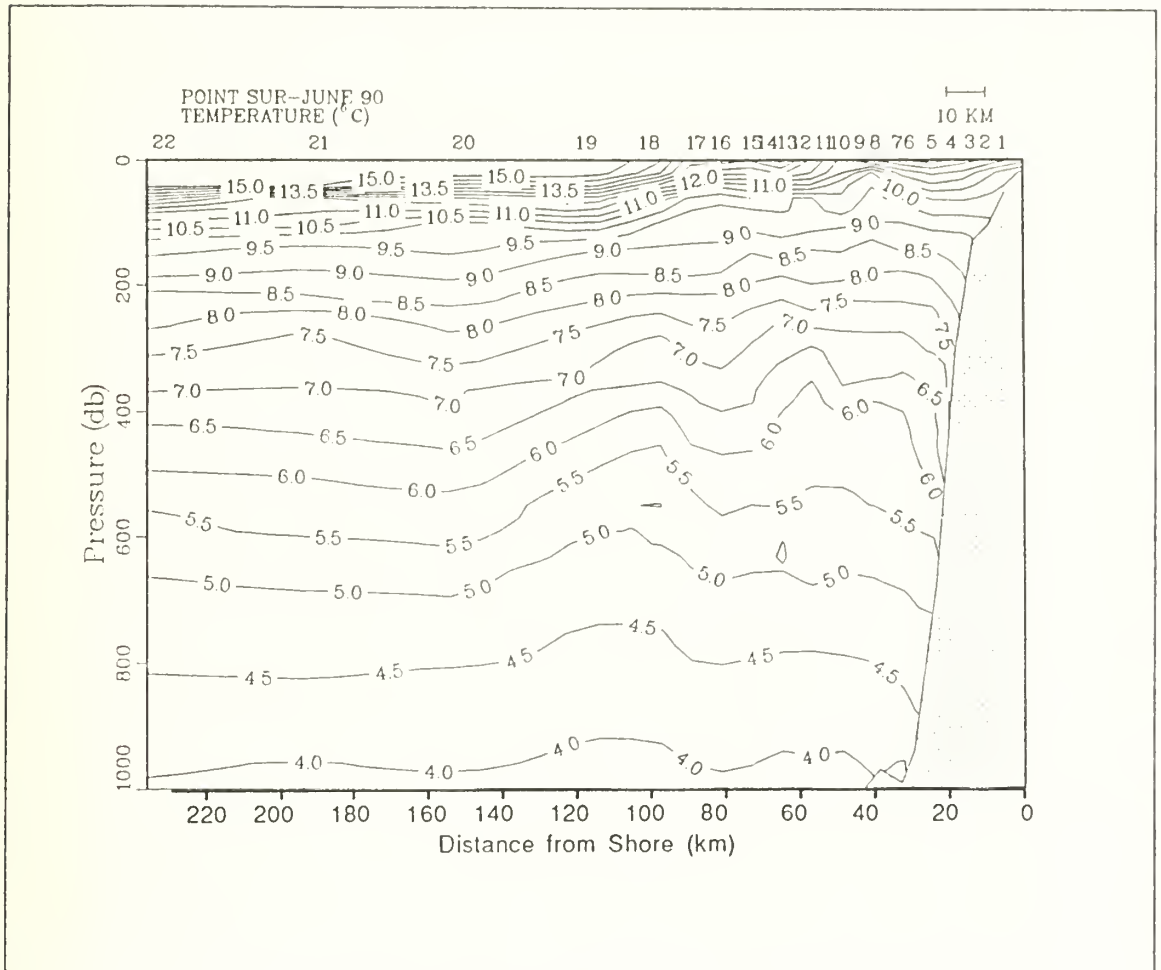
18

Figure 5. Spatial variation of temperature

- Except at the coast, relatively colder water can be distinguished between Stations 1 and 9 from 100 dbars to a depth of 600 dbars; above 100 m, a lens of warmer water is found.

- From Station 9 to Station 11 the isotherms bend upward showing a cold water mass at the surface, coming ultimately from greater depths.

- Between Stations 11 and 16 warm water core can be distinguished in the upper layers.

- Between 500 and 1000 dbars there is a "ridge" of cold water at Station 18 which separates warm inshore water from warm offshore water.

- Close to the shore strong upwelling occurs in the upper layers above to the depth of 130 dbars.

- "Deep waters zone" This zone includes the waters below 1000 dbars. At this zone the horizontal temperature remains almost the same for all the stations and a rather strong layering of the water is observed. This can be concluded by the fact that the

isotherms are almost horizontal and as the depth increases the temperature gradient becomes smaller.

Temperature variability between station pairs decreases with depth. For some station pairs the above rule fails in that the differences in temperature between the stations are greater at greater depths giving an idea that these stations are the limit of two different water masses.

3. Salinity

Vertically, salinity in general increases as the depth increases. Horizontally salinity varies as follows:

- "Surface zone" (Surface to 100 dbars) From Station 1 to Station 5 (Figure 7) salinity decreases showing minimum at Station 5. Further offshore to Station 9 salinity increases showing maximum at Station 9. Station 9 is the center of a local salinity high between the fresh offshore water and the fresh water centered at Station 5. Westward from Station 9 until Station 18 salinity decreases presenting minimum value at station 18. From Station 18 to Station 22 salinity increases slightly. In general the water mass landward from Station 9 is salter than that offshore from Station 9. As in the temperature case, the salinity isohalines present upward sloping close to the shore starting from a depth 130 dbars. This means that salty water rises from this depth close to the shore and amplifies the assumption of upwelling.

- "Halocline" (100 to 1000 dbars). The picture is almost the same as in the surface zone with the difference that the changes of the salinity are not so large in magnitude. Horizontally in this layer we can distinguish two salinity peaks. One is at Stations 8 and 9, between the surface and 200 dbars, and the other at Station 16 between 200 and 1000 dbars. A relatively large horizontally salinity variability occurs between 300 and 600 dbars landward of Station 15. This gives the idea that strong current shear may occurs at these depths. At depths greater than 130 dbars isohalines slope downward when close to the shore.

- "Deep waters zone" (1000 to 4000 dbars). Here the isohalines are almost horizontal presenting strong layering and the changes of the salinity with the depth are very small. No sloping of the isohalines is observed when these close to the shore as in the previous zones.

The positive saline gradient with depth is greater at the upper 200 dbars and especially close to the shore, and becomes smaller as the depth increases. Salinity difference between the stations pairs (Figure 8) closes to zero after a depth. This may give an idea where strong motion of the water masses occur, or where the level of no motion is. This depth varies and it is observed that going offshore the depth where the difference closes to zero increases.

4. Density

From density profiles of the Stations (Figure 9) it is observed that denser water exists closer to the shore and lighter offshore.
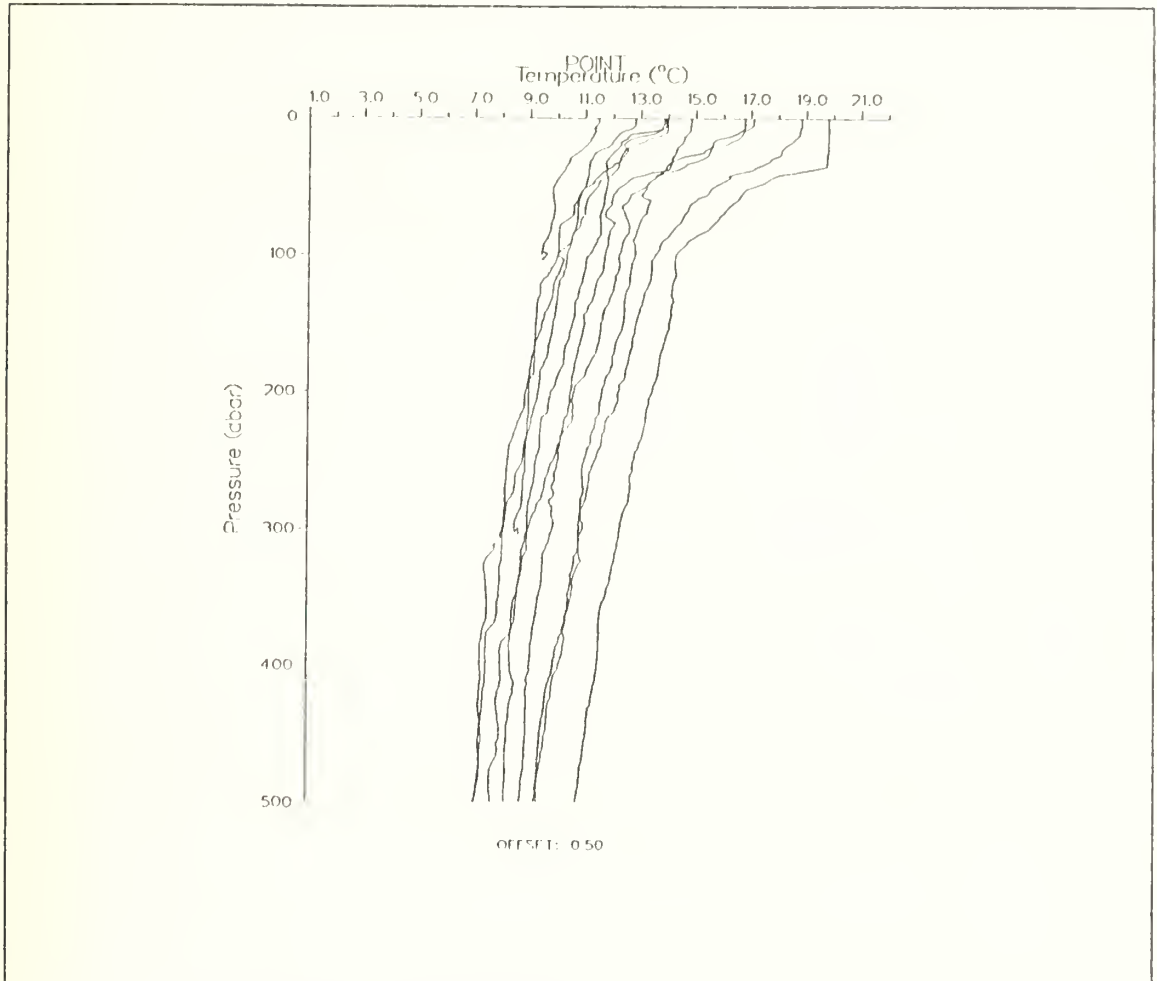
Figure 6. Mixed Layer Depth variation

Describing the density profile of the stations in the same way as for temperature
and salinity, we have:

- "Surface zone". From Station 1 to Station 9 we observe first a decrease of the
  density until Station 5 and then an increase until Station 9. A surface density
  maximum is located between Stations 8 and 9 which indicates a surface velocity
  shear. Offshore from Station 9 to Station 19 there is a continuous decrease of
  density. This gives the idea that water masses of different characteristics flow in the
  area. Beyond Station 20, the upper layer density is quite homogeneous. Concluding,
  in this zone the denser surface water exists close to the shore and the lighter off-
  shore.

- "Pycnocline". As in the upper zone, in this zone the denser water is generally close
  to the shore and the lighter offshore. Between 130 and 800 dbars the isopycnals
  slope upward toward the east except immediately adjacent to the bottom. Below
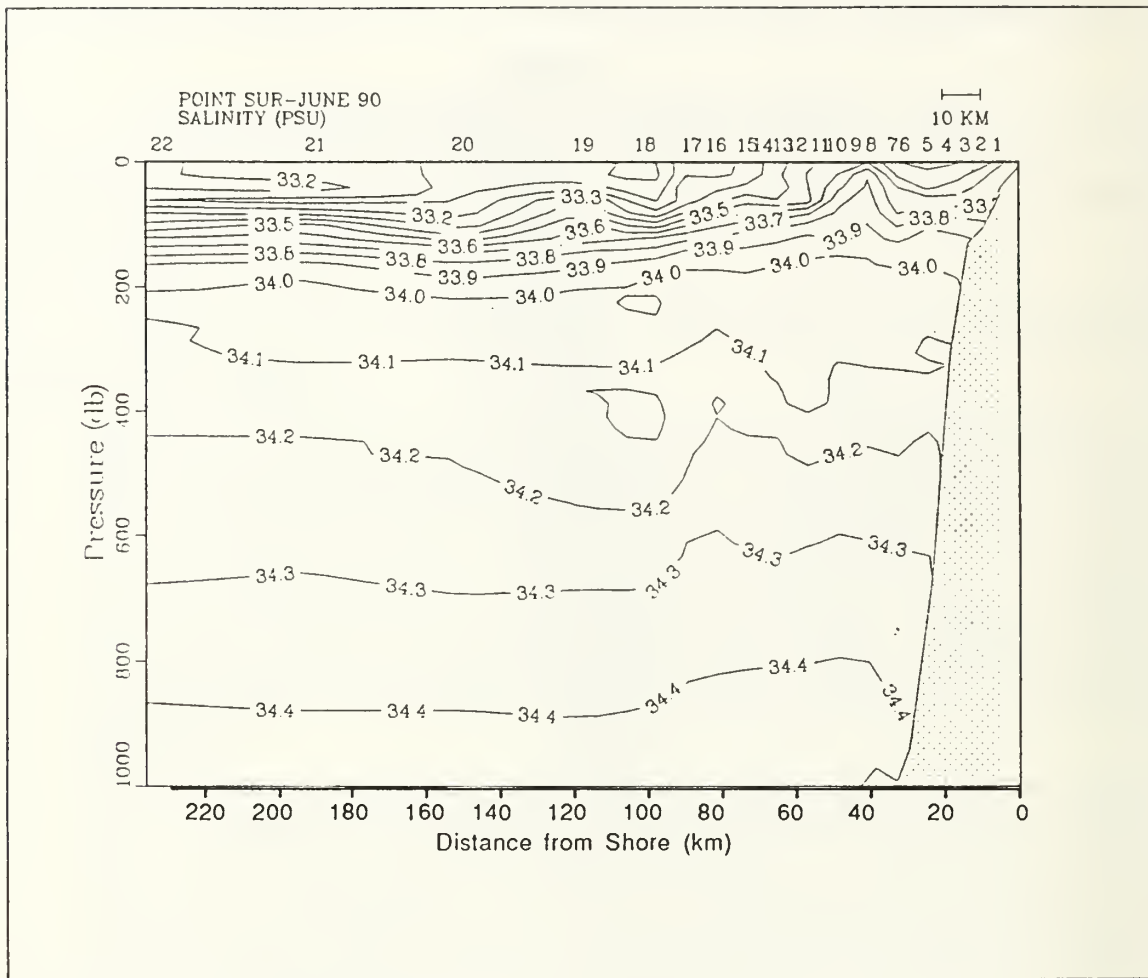
21

Figure 7. Salinity distribution

800 dbars the isopycnals are increasingly horizontal. In general in this zone density reveals the same trend in variability as in the previous zone with smaller magnitude.

- "Deep waters zone" Below 1000 dbars the isopycnals are almost horizontal and the density gradient very small.

Looking at the whole picture we see that in the upper layers the density gradient with depth is large. As the depth increases the positive density gradient decreases and below 1000 dbars the gradient becomes almost zero.

5. Temperature/Salinity characteristics

Because the water masses mix with the surrounding waters very slowly, they tend to retain their original temperature and salinity. The distinctive temperatures and
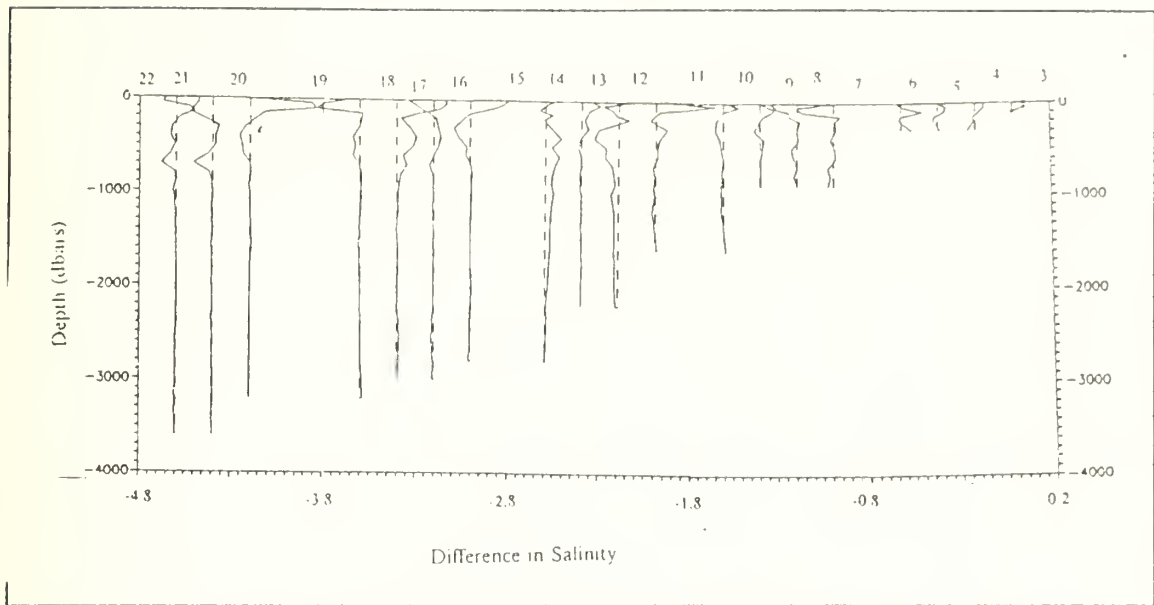
Figure 8.   Salinity differences between the stations in pairs

salinities of these masses make it possible to identify them. The identification gives us information on their place of origin and the rates at which waters of different origin mix.

The T/S diagram generated using the data from June 1990 (Figure 11) can be studied, again by using distinct depth zones.

- The first zone ranges from the surface to 150 dbars. This zone includes the water lighter than density anomaly (γ) 26.2 kg/m³. As can be seen in the diagram at the surface we can distinguish two different water masses, one between Stations 1 and 15 and the other between Stations 16 and 22. The denser and colder water is at stations closer to the shore and the lighter and warmer offshore. In the upper 100 dbars more stable water lies at Stations 1 to 16 and less at Stations 20 to 22.

- The second zone ranges from 150 to 300 dbars (26.2 to 26.6 kg/m³). At this zone the water masses of all the stations present almost the same characteristics and have the same stability.

- Proceeding deeper to the third zone for 300 to 700 dbars (26.6 to 27.2 kg/m³) the picture from the T/S diagrams is more complicated and interesting. At 400 dbars Stations 12 and 13 present colder and less saline water than all the other stations. From 400 to 700 dbars Stations 17 and 18 present colder and less saline water in all the range of the depth. Water mass of stations 12 and 13 is less stable than the water mass of the other stations and at Stations 17 and 18 more stable than all the other stations.

- Deeper than 700 dbars the water mass of all the stations has the same characteristics and stability in all the range of depth.
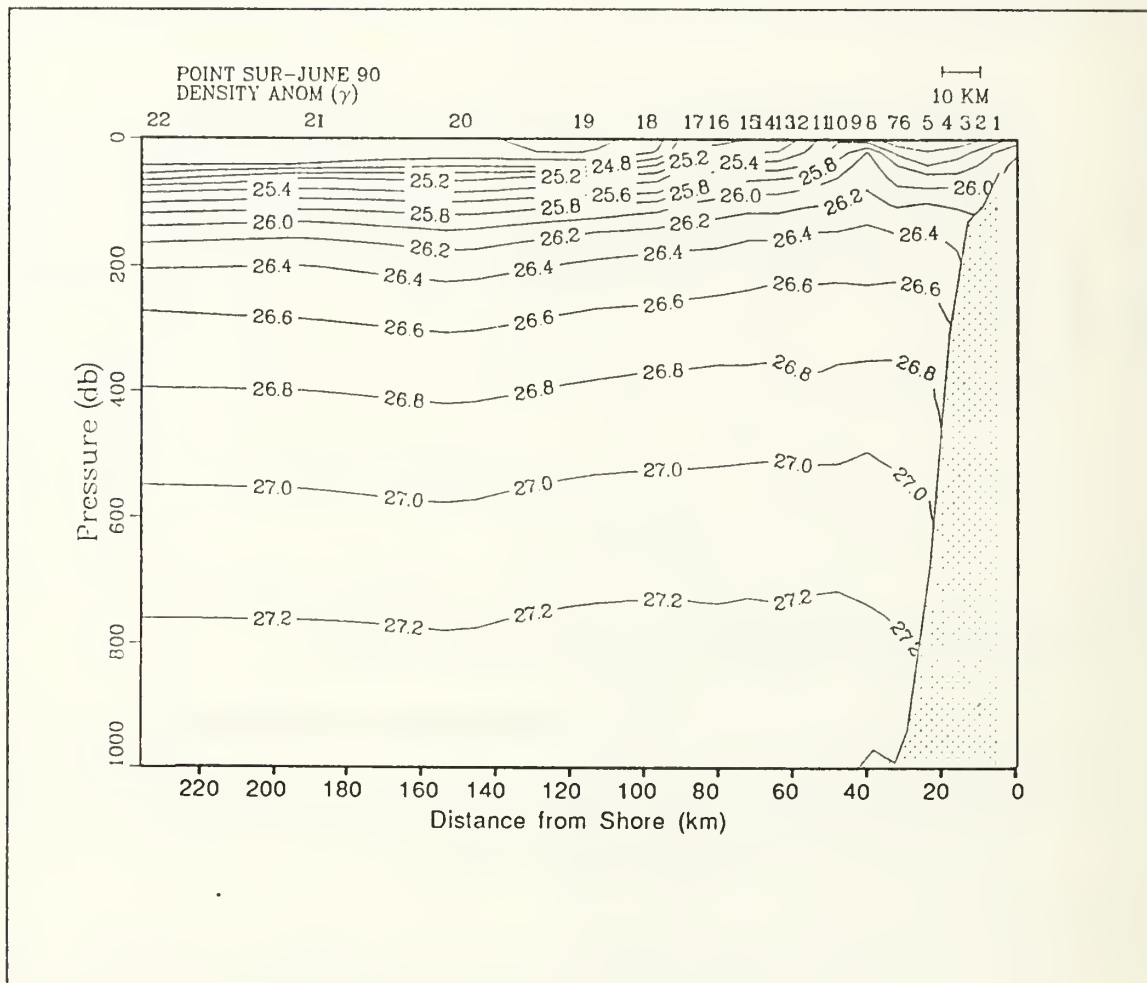
23

Figure 9.   Spatial distribution of density

Relating these observations with the water masses refered to in a previous paragraph and Tables 3 and 4 we have:

- In the upper zone (0 to 150 dbars) North Pacific Subarctic Water mass mixing with North Central Pacific water is shown. Stations far offshore show greater temperature due to location and remoteness from coastal phenomena (upwelling).

- Subsurface water, signified by the salinity high near the shore and more uniform at depth, causes the bend of the T/S curves to the right. Small variations in salinity and temperature at some stations is observed which make the picture more complicated. Stations 12 and 13 show colder and less saline characteristics at the depth of 400 dbars and similarly at Stations 17 and 18 in the range 400 to 600 dbars. The presence of this variability suggests a complex flow regime.

- Deeper than 700 dbars Deep Water dominates in all the range of the depth.
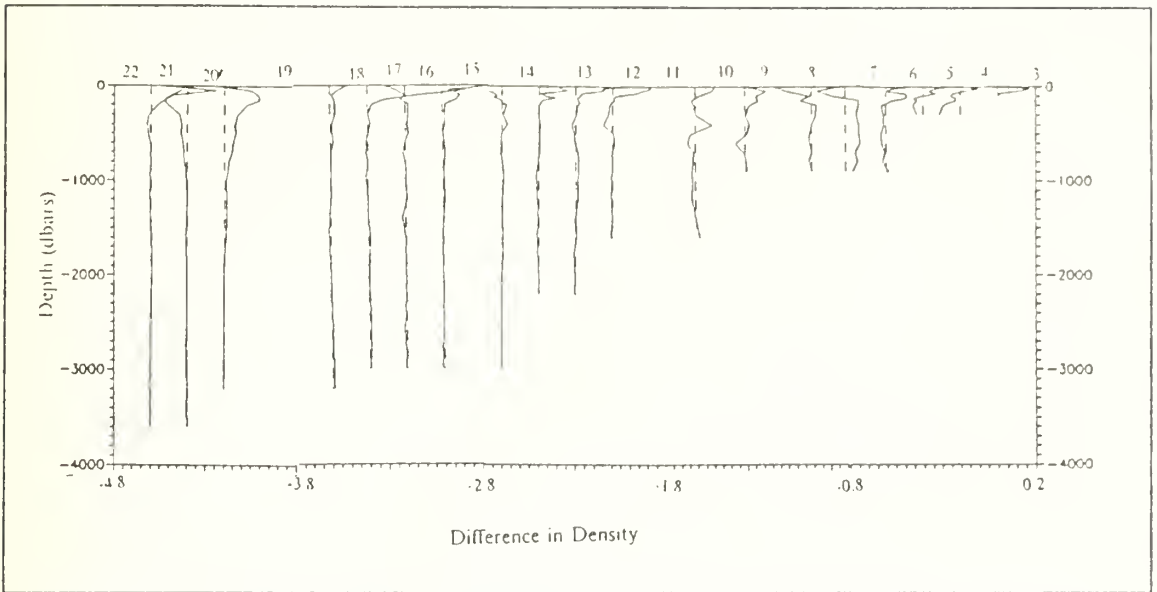
Figure 10.   Density differences between the stations in pairs

6.   Spiciness

The following paragraph of the definition of spiciness was taken from Tisch (1990).

"Spiciness $\pi(\theta, s)$ is the state variable which is most sensitive to isopycnal thermohaline variations and least correlated with the density field (Flament 1986). Spiciness is useful for the description of interleaving and double diffusive processes which occur at the boundary between different water types. Waters which are warm and salty have positive π values while those which are cool and fresh have negative π values".

From station 1 to station 22 in the upper 50 dbars the spiciness has positive values. The positive scale of the spiciness, ranges from 0 to 0.7, with the greatest values on the surface and far offshore (Station 22). The high temperature on the surface at stations far offshore from Station 15 is the reason for positive spiciness values until the depth of 50 dbars although low salinity water flows in the area. At greater depths the spiciness profile has negative values below the depth of 50 dbars. Below 50 dbar, a lens of negative spiciness exists at some stations. However, at 200 dbar, a layer of positive spiciness is found again. This layer shoals toward the coast with a tilt similar to the isopycnals, reflecting coastal upwelling. At depths greater than 300 dbars and in all the range offshore (Station 1 to Station 22) only negative values of spiciness are shown. Between 300 and 600 m, large variations in the depth of the -0.1 spiciness occur inshore
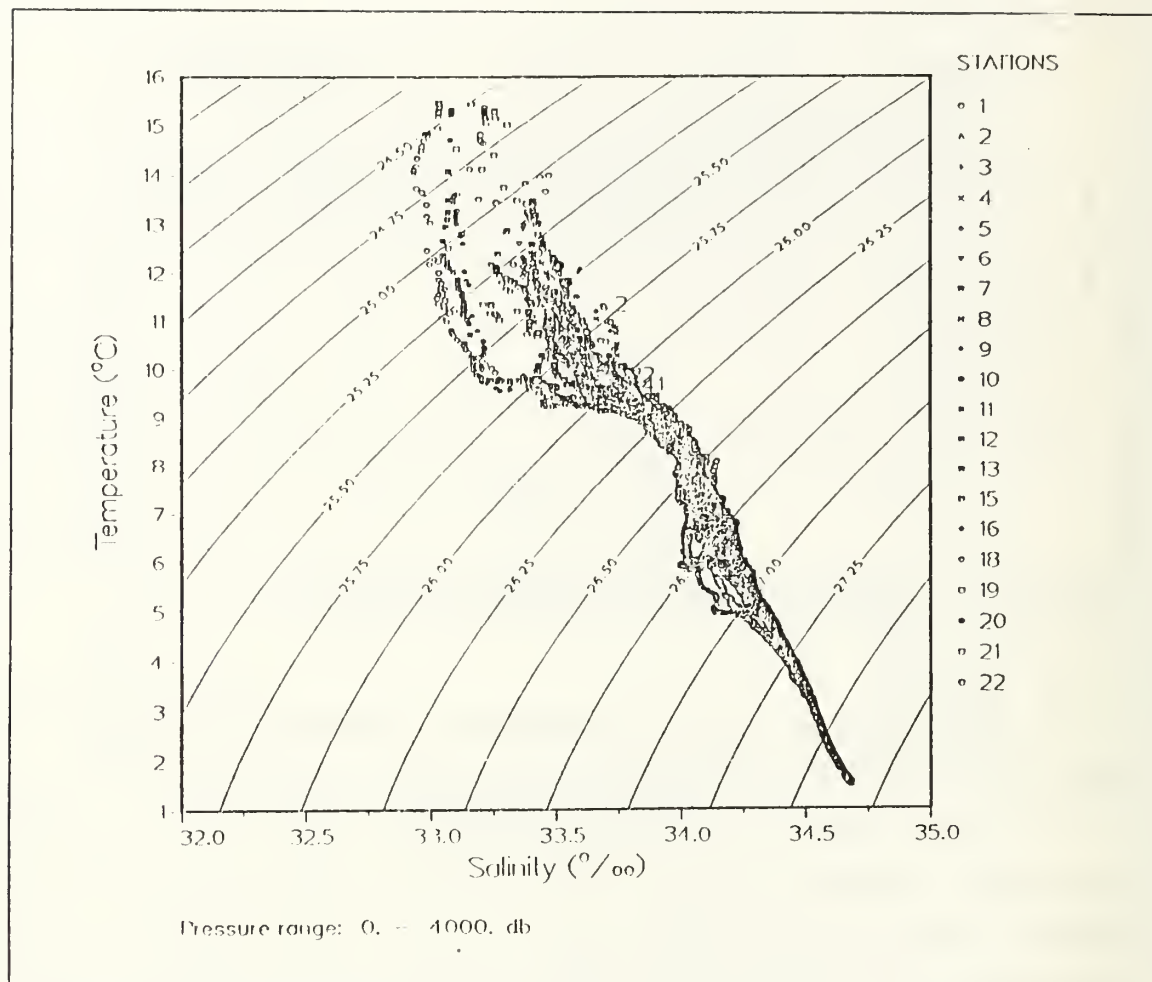
25

Figure 11. T/S characteristics

of station 18. This indicates the discontinuous character of undercurrent waters noted in the above discussion of T/S properties.

7. Level of no motion

Parts of the following theoretical description of the LNM are copied from Fomin (1964).

a. Defant's method

Although there is not a universal objective method for determining the layer of no motion, I tried to find the level of no motion by Defant's method (1941). According to this method, which is a method used in the open ocean, the level of no motion or the level where the current's speed is very small, is determined by differencing the

Figure 12.   Spatial distribution of the Spicines
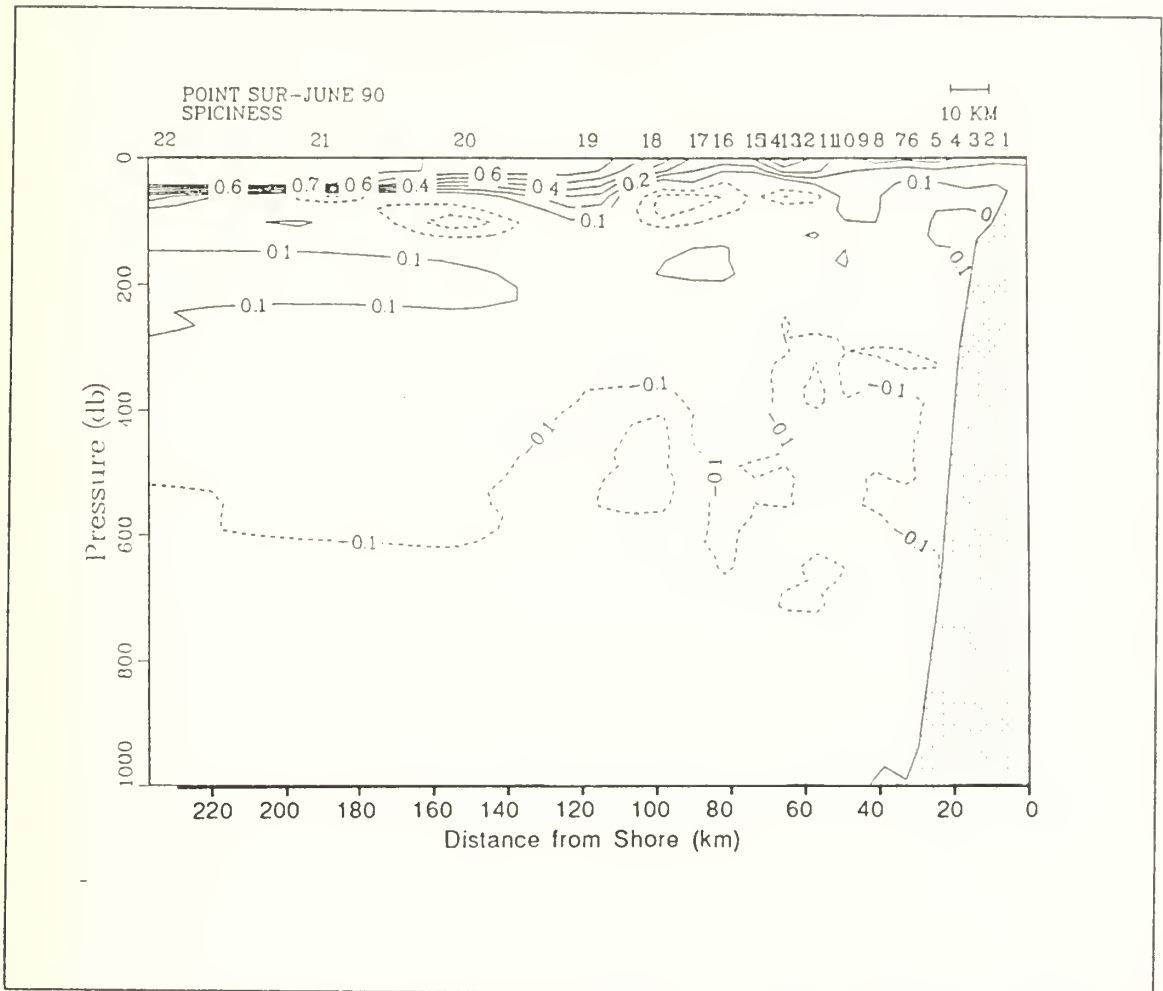
dynamic depths of isobaric surfaces at a great number of pairs of neighboring stations.
"The constancy of differences in dynamic depths indicates that the gradient component
of current velocity is constant along the vertical in that layer." By Defant's method it
is accepted that the depth, or the range of the depth, where the differences in dynamic
depths are constant is the layer of no motion. "Indeed, the curve for the vertical dis-
tribution of differences in the dynamic depths of isobaric surfaces is identical with the
curve for the velocity component of the gradient current that is normal to the profile.
It is sufficient to multiply the difference in dynamic depths by $(2\omega L sin\phi)^{-1}$ to obtain the
velocity of the gradient current with an accuracy to the constant value. This constant
value is equal to current velocity at the sea surface. So Defant's method of determining

27

the "Level of No Motion" is based on analysis of the vertical variation of the velocity of the current being computed by the dynamic method."

b.   *Open ocean assumption*

"The strict constancy of differences in the dynamic depths of isobaric surfaces of some depth interval means that the increments in dynamic depths between two levels are equal at two neighboring stations i.e.

$$\Delta D_A = \Delta D_B \tag{1}$$

or

$$[\int_{P_n}^{P_{n+1}} \alpha dp]_A = [\int_{P_n}^{P_{n+1}} \alpha dp]_B \tag{2}$$

where:

- ΔD_A and ΔD_B are the increments in dynamic depths between the isobaric surfaces p_n and p_{n+1} at stations A and B and

- α is the specific volume of sea water.

"Geometrically the above equation means that the areas formed by the curves for the vertical distribution of specific volume between surfaces p_n and p_{n+1} are equal at stations A and B. Hence there is at least one depth in the (p_n, p_{n+1}) interval where the specific volume of water is the same at stations A and B. If the distance between hydrological stations is small there is at least one horizontal isostere in the $[p_n, p_{n+1}]$ interval and the slopes of the isosteric surfaces must be opposite in sign above and below it."

c.   *Results for data of June 1990*

Figure (13) shows the vertical distribution of the differences in dynamic depths of isobaric surfaces along the Point Sur Transection. The arrows designate layers with similar differences in dynamic depths, suggesting the reference layer depth.

As we can see from the graph, the selection of the depth of the layer of no motion is somewhat uncertain. Close to the shore the depths where similar differences occur are shallow (less than 700 dbars), further offshore the depth increases and in some cases becomes greater than 1000 dbars.

The first two curves (differences in dynamic depths between Stations 4 and 5 and 5 and 6) show great change with depth, which means that the change of the cur-
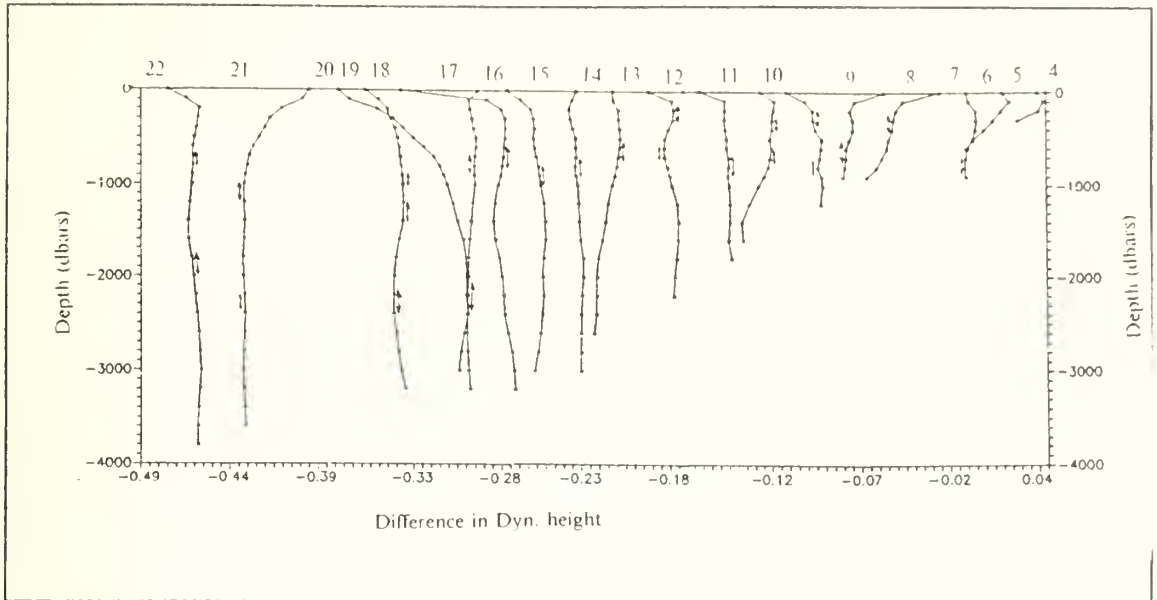
Figure 13.   Differences in dynamic heights of neighboring stations. The arrows
              designate where the vertical gradient of dynamic depths are similar be-
              tween stations.

rent velocity with depth is large. The curves offshore from Station 8 exhibit a slight
change with depth except between Stations 10 and 11 which show remarkable change
at depth 800 dbars. The above lead to the assumption that Stations 4, 5, and 6 lie on
the main stream of a current flowing northward whose the velocities will be discussed
later in the geostrophic's velocity section. Offshore from Station 8 we expect slight
change in the velocities (mainly at depth) and a northward core at Stations 10 and 11 in
depth.

In many cases, as it is shown in Figure 13, we have more than one depth
where the layers with similar differences in dynamic height occur. According to Defant,
in this case the investigator has to decide the correct depth of LNM. In my case, I
checked the the dynamic height differences between the stations in pairs with the
Pegasus and ADCP results. I decided that a LNM between 500 and 600 dbars it is the
most appropriate to be used to study the undercurrent close to the shore. This LNM
cannot give good results if we want to check the currents further offshore. In this case
a LNM greater than 700 (800 dbars looks to me most appropriate) has to be used. To
get better picture of the current's velocity in the area using only one LNM for all the
stations, I decided to use LNM 700 dbars. In this depth most of the differences show

29

constancy with depth and the Pegasus results give zero V velocity. I believe that landward of Station 9 the use of 500 dbars as LNM gives better picture of the under-current. Offshore from Station 9, use of 800 dbars gives the better picture.

d. Differences in density between the stations

Another way to estimate the LNM is from the difference in density between the stations pairs. It is based on the same principles of the Defant's method and it comes through the theory which it is described in detail in Fomin (1964). The result is that the LNM can be estimated to be the depth where the horizontal pressure gradient between stations is zero.

Following the above I tried to find the depths where the difference in density between the station pairs is equal to zero. I found that going offshore the depth where the difference of density closes to zero increases. Landward of station 8 the depth where the difference closes to zero lies between 400 and 600 dbars, further offshore ranges between 800 and 1100 dbars.

Comparing these results with the results from the Defant's normal method (differences of dynamic height), I decided that the level of no motion for the Stations 1 to 8 is about 600 dbars and for the stations further offshore, 800 to 1000 dbars.

e. Salinity variation between the stations in pairs

The above results become more reliable when we compare these with the salinity distribution. If we take into mind that the water velocity shear causes salinity variations and, from the other side, motionless water usually is homogeneous, then taking the differences in salinity between the stations in pairs we get about the same results as above.

The depth where the difference in salinity closes to zero landward of Station 8 is about 400 to 700 dbars, at stations offshore from Station 8, 800 to 1100 dbars. Most of the stations show a depth 600 dbars. So based on all the above I decided to use as LNM 700 dbars as the most representative for the area to proceed finding the geostrophic velocities.

8. Dynamic topography

a. Dynamic topography for 500 dbars

For the first 4 stations the programs didn't give dynamic height values. Further offshore "High" and "Low" occur as are shown in Figure 14. From Station 5 to Station 9 (23 - 42 km) the dynamic height decreases giving the lowest value at Station 9 (42 km). Offshore from Station 9 the dynamic height increases giving the highest value at Station 20 (150 km). According to the above we can say that landward of Station 9
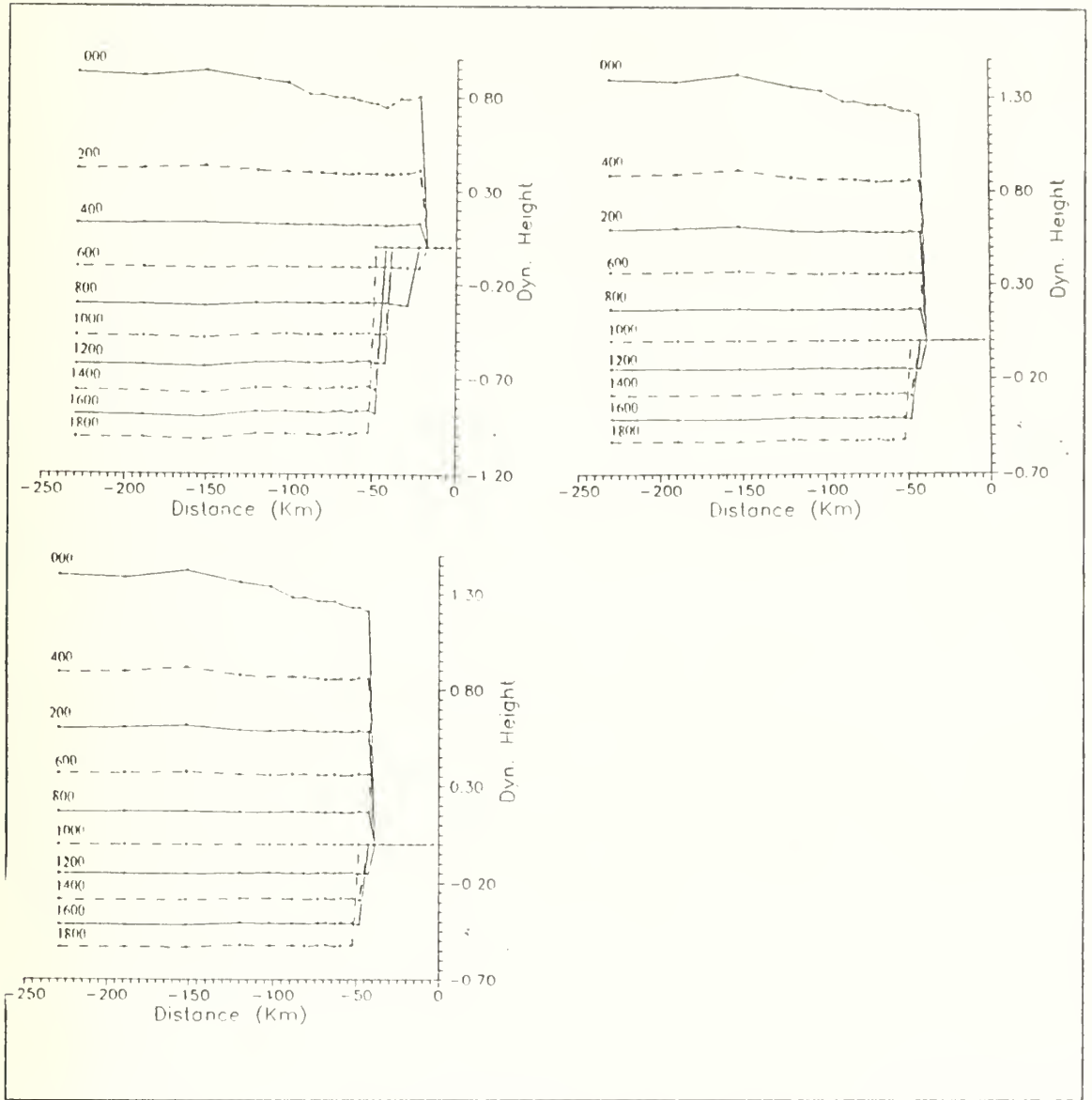
30

Figure 14.   Dynamic topography for LNM 500, 700 and 1000 dbars

we expect flow going northward whose the velocities will be given in the geostrophic velocities plots. Station 9 it is expected to be the limit of two different flows. Due to continuously increasing of the dynamic height values offshore from Station 9 a broad southward current it is expected until Station 18 (100 km), and southeastern until Station 20. Further offshore to Station 21 (190 km), the direction of the flow is expected to change to the northwest.

31

b. Dynamic topography for 700 dbars

For the first 5 stations the DYNHGT program didn't give values of the dynamic height because the stations are too shallow for the LNM 700 dbars. From Station 6 to Station 9 (29-43 km) the dynamic height decreases showing the smallest value at Station 9. Further offshore from Station 9, the dynamic height values increase giving the highest value at Station 20 (150 km). From Station 20 to 21 (190 km) the dynamic height values decrease. To connect this changing of dynamic height with the water flows which we expect, we can say that from Station 6 to Station 9 we expect a northward current whose the offshore limit is at Station 9. Further offshore to Station 20 we expect a broad southward current and more offshore to Station 21 a northwestern flow.

Taking into account the dynamic height differences between the station pairs we expect the core of the northward current close to the shore to be between Stations 5 and 6 (23-29 km). The velocities of this current will be given later geostrophic velocities section.

c. Dynamic topograghy for 1000 dbars

Until Station 8 (38 km) no dynamic height can be computed because the stations are too shallow for the used LNM. Further offshore the dynamic height of the stations increases with the highest point at Station 20 (150 km). According to the above, from Station 9 to Station 18 (42-102 km) we expect southward flow. Between Stations 18 and 20 (102-150 km) southeastern flow and between 20 and 21 (150-190 km) northwestern. The important information which is given in this graph is that the lowest value of the dyn. height still remains at station 9 so this station can be accepted as the landward limit of the broad southward current.

9. Velocities

a. Geostrophic Velocities

When high pressures are on one side and low pressures on the other, motion of the water starts from high to low. As the motion starts the Coriolis force acts and deflects the water to the right in the northern hemisphere. As the water is deflected the Coriolis force will always be perpendicular to the new deflected motion and turning of the current will continue until the Coriolis force opposes and balances the downhill component of the gravity force. When this stage is reached the water will move along the topographic contours and geostrophic motion has been generated. This geostrophic motion will continue indefinetely if friction is absent. Profiles of the geostrophic velocities have been drawn for 3 levels of no motion as follows.
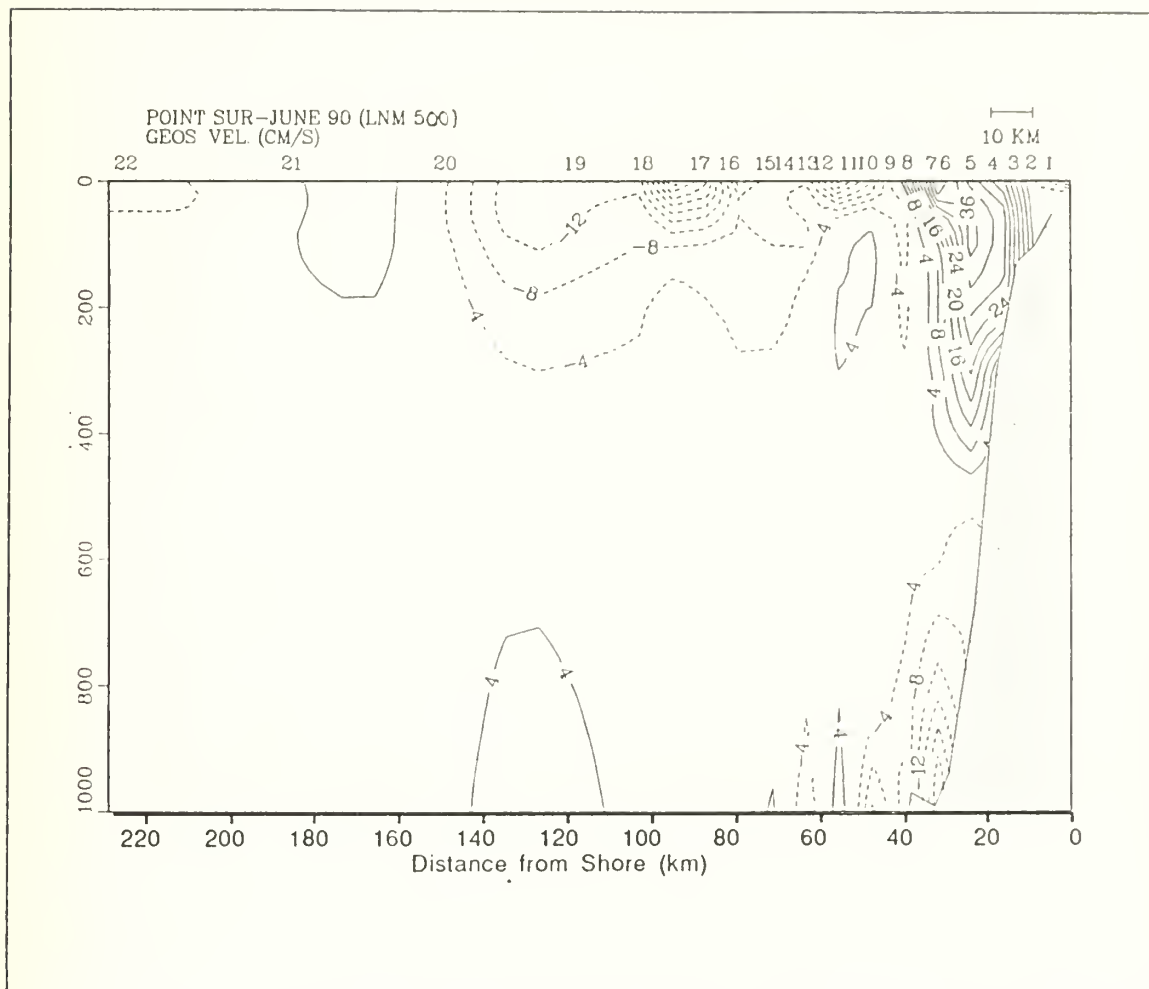
Figure 15. Geostrophic velocities for LNM 500 dbars

- Geostrophic velocities for LNM 500 dbars.

    The big picture includes a northward flowing current close to the shore and a southward current offshore from Station 9. Further offshore from Station 18 southeastward flow it is shown which actually is the southeastward component of the southward current which is mentioned before.

    The greatest depth to which the currents extend and the speed of the currents with depth vary as follows. The northward flowing current close to the shore presents the greatest speed at a depth 150 dbars and it is 36 cm sec. The northward flow penetrates to 500 dbars between Stations 4 and 5. The southward flowing current shows the greatest speed at the surface (between Stations 11 and 12 and Stations 17 and 18) and 36 cm/sec. It is a shallow current and its greatest depth is 300 dbars.

- Geostrophic velocities for LNM 700 dbars. From Station 2 to Station 9 a northward current is shown. The core of this is located at Station 5 and the maximum velocity 36 cm/sec. Offshore from Station 9 a broad southward current is
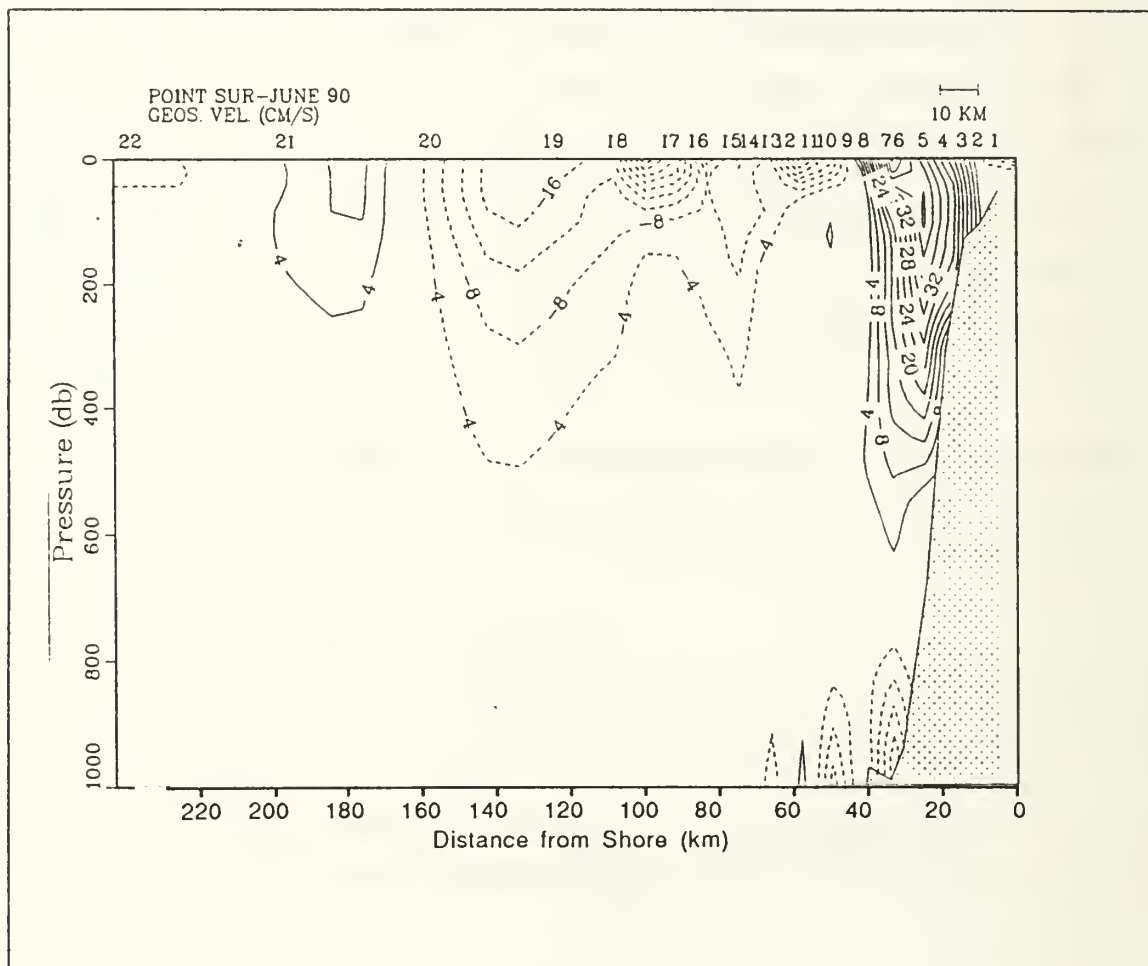
33

Figure 16.   Geostrophic velocities for LNM 700 dbars

shown whose the maximum velocity is 32 cm/sec and extends until Station 18. Due to the change in the orientation of the line of the casts from Station 18 to Station 20 a southeastern current is shown which actually is the southeastern component of the previously mentioned southward flowing current. Offshore of Station 21 a northwestern flow is shown which is restricted in the upper 300 dbars.

- Geostrophic velocities for LNM 1000 dbars.
  As in the previous case the big picture for LNM 1000 dbars is a northward flowing current close to the shore until Station 9 (43 km offshore) and a southward current offshore from Station 9 to Station 18. Further offshore southeastward flow is shown until Station 20 and northwestward until 21. The southeastward flow actually is the southeastward component of the southward flow mentioned before.

      Greatest speed of the northward flowing current is 44 cm/sec, at 150 dbars and the greatest depth 800 dbars. The southward flowing current shows greatest speed 32 cm/sec at surface and greatest depth 900 dbars.
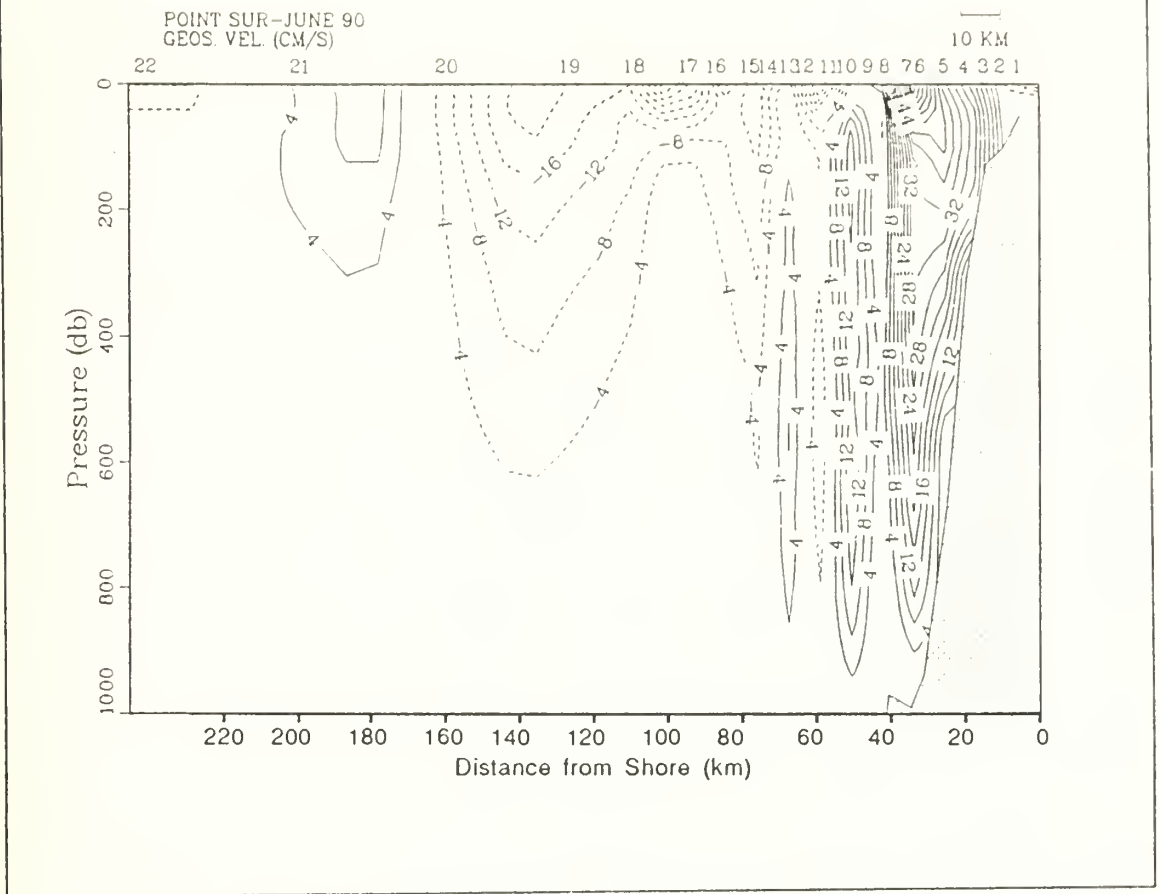
Figure 17.   Geostrophic velocities for LNM 1000 dbars

All three LNM give about the same picture; a relatively strong northward flow close to the shore and a southward flow further offshore of Station 8 or 9. Trying to compare the results from the three used LNM, we see that as the depth of LNM increases stronger northward velocities are shown close to the shore. More, as the depth of the LNM increases the northward flow is shown wider reaching to a distance 72.5 km offshore (Station 15). The results from these have to be compared with the results from Pegasus, ADCP and AVHRR for better results.

Something which wasn't mentioned in the three geostrophic profiles, but which is present in Figure 16, is the southward flowing coastal jet. This is the result of the strong favorable for upwelling winds and it is restricted close to the shore. It pre-

35

sents its maximum speed at surface which is 10 cm/sec. It is a very shallow current carrying mainly cold upwelled waters.

b. *Pegasus Velocities*

(1) *V Velocities.* As was mentioned in a previous paragraph, the starting point of Pegasus survey is 33 km offshore. The first seven stations start from $36°20.12$ N and $122°16.22$ W and extend westward, laying on the same parallel and are at 10 km intervals. This arrangement gives the advantage for better covering of the area closer to the shore and the chance to study the current close to the shore.

To study the currents in the area with Pegasus, I found the V velocities first for the drops 258, 259, 262, 263, 266, 268, 269, 272, 274 (first run) and second for the drops 260, 261, 264, 265, 270, 271, 273, 275 (second run).

To examine the relationship of the V velocities in each station for the first and second run in the upper 400 dbars, I averaged the V velocities in bins of 20 dbars and examined the mean and the standard deviation of the V velocities horizontally. As it was expected the the greatest northward mean velocities occur close to the shore. Offshore from Site C4 the mean velocities are southward until Site C9. Site C9 shows again weak northward velocities in all the range of the depth (400 dbars). The greatest values of standard deviation occur at sites close to the shore and upper layers and the smallest offshore. This gives an idea that the northward undercurrent close to the shore experiences great V velocity variations caused by different forces, as for example inertial motion, winds, internal waves, tidal waves, etc. Current meters data for the same period show that the inertial motion can cause variation of the California Undercurrent's velocity of up to 4 cm/sec. Tidal constituents can affect the current's velocity up to 6 cm/sec (Sielbek, personal communication). Taking these information into account, we can justify somewhat the large values in standard deviation. But I believe that further study of the problem with current meters data is needed for better results. Of course in these high standard deviation indications we cannot exclude the device's errors and position errors (different position of measurement in the first and second run).

The average velocity of the two runs should cancel some of the effects from all the factors which cause the variations and give a more integrated picture of what happens in the area. Figure 18, which gives the average velocity cross section, shows details of three flow regimes. Poleward flow is shown in the upper 700 dbars until the distance 72 km offshore. This current is strongest at the upper layers (almost the surface) and weakens as the depth increases. The maximum speed of this is 32 cm/sec, the core of which is located at a depth 40 m.
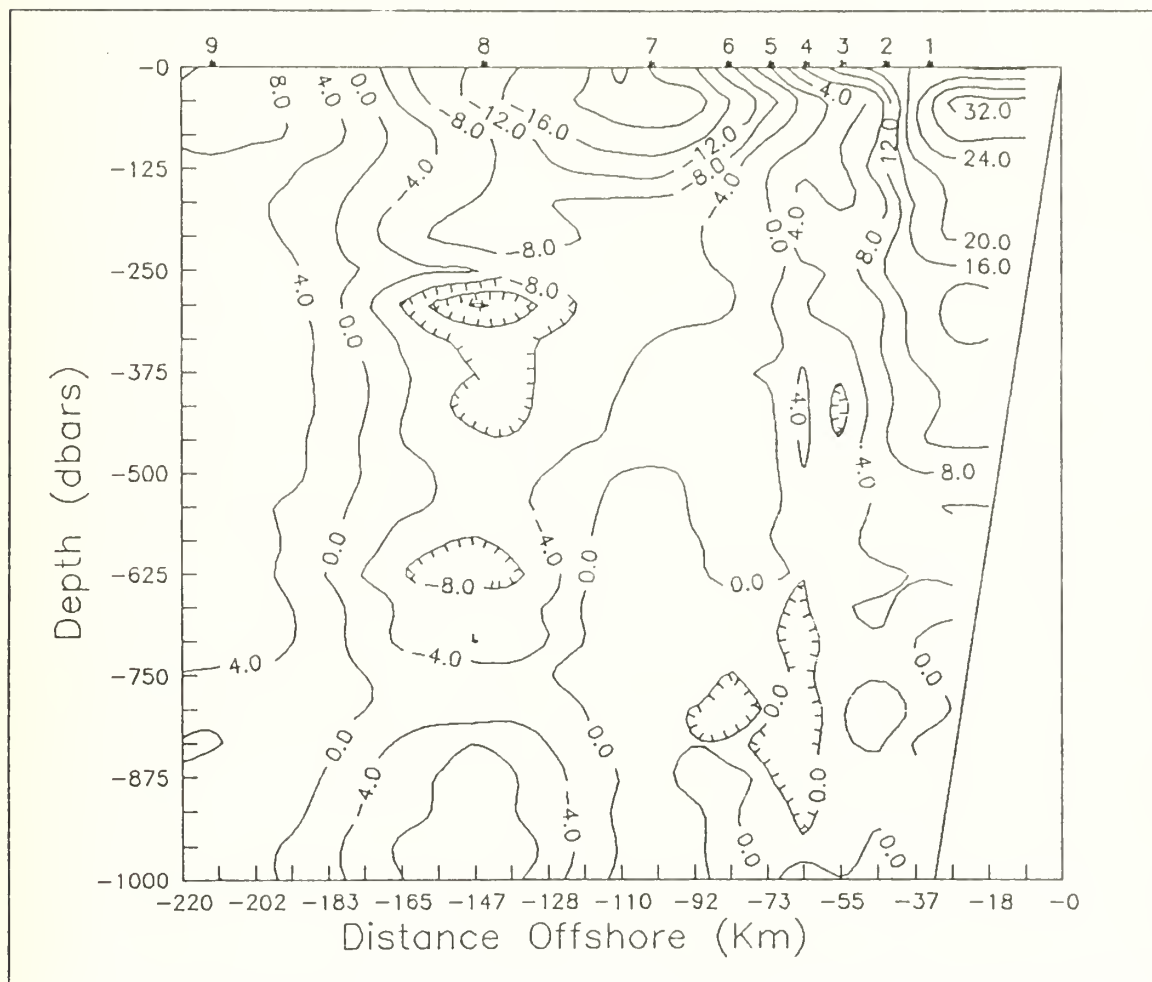
36

Figure 18.   Pegasus V Velocities. Average velocities of the runs

Offshore from Pegasus Site C5 (72 km) to Site C7 an equatorward flow is shown in the upper 1400 dbars. The greatest velocities are on the surface. The core of this flow is located at 102 km offshore and the greatest speed is 24 cm/sec. The southward flow extents to a distance 180 km offshore.

Further offshore from 180 km the flow becomes northward but the speed of this does not exceed to 10 cm/sec. The vertical extent of this far offshore poleward flow is 800 dbars. At depths greater than 1500 dbars the alongshore velocities are southward and in most places are almost zero.

Relating these results with Chelton's suggestions (alongshore geostrophic velocities at 150 dbars < 10 cm/sec and southward flow during June), we

conclude that the velocities in this case are much different than that of Chelton's, who suggested southward flow during this period. Comparison of these with the geostrophic velocities for LNM 700 dbars discussed before, gives the same picture. Strong northward flow close to the shore and southward less strong flow offshore from Station 9. At depth the northward flow close to the shore flow extends further offshore to Site 12. Comparing these results with the geostrophic velocities of previous studies of NPS students for about the same period, (Table 2) it is observed that these velocities are higher.

Figure 19 gives the cross section of V velocities for the first and second run and the opportunity to check for the differences or similarities between the two runs. The first run shows a strong northward flow close to the shore extending 83 km offshore and at a depth 650 dbars. The greatest speed of this is 32 cm/sec at a depth 50 dbars. At distances greater than 83 km offshore, a southward flow is shown which extends until 190 km offshore. This southward flow looks slower than the previous northward, but wider and shallower. The greatest speed of this is 24 cm/sec on surface and decreases downward. Some southward and relatively strong cores appear to be generated at depths but below 1500 dbars all these diminish so at greater depths no motion is shown. Further offshore from 190 km northward flow appears with small velocities (smaller than 8 cm/sec). These northward velocities extend downward to 800 dbars. Deeper than this depth weak northward cores appear in all the range of the depth (4000 dbars).

As in the first run, second run shows a strong northward flow close to the shore extending at the surface 95 km offshore. This northward flow is strong in the upper layers and weakens as the depth increases. The greatest speed of this flow is 32 cm/sec at a depth 30 dbars and closes to zero at a depth 700 dbars. From 95 km offshore to 190 km offshore a southward flow is shown. This southward flow is stronger at the upper layers and weakens as the depth increases. Maximum velocity of this flow is 28 cm/sec at a depth 30 dbars and weakens as the depth increases. Some cores of stronger southward flow are shown at depths greater than 500 dbars to 1300 dbars, which diminish after 1300 dbars. Offshore of 190 km northward flow again is shown with smaller velocities than the previous two flows. This northward flow extends downward to a depth of 1000 dbars, at greater depths no water motion is shown.

Both cross sections show clearly the California Undercurrent flowing northward with the core located at a distance less than 33 km from the shore and depth 50 dbars. The width of the northward flowing undercurrent on the surface in the second run is greater than the first leading to the assumption that external forces as the wind
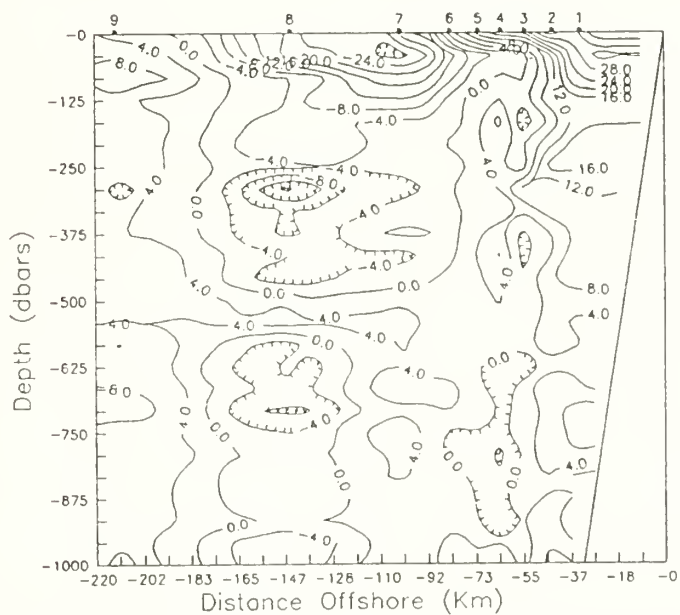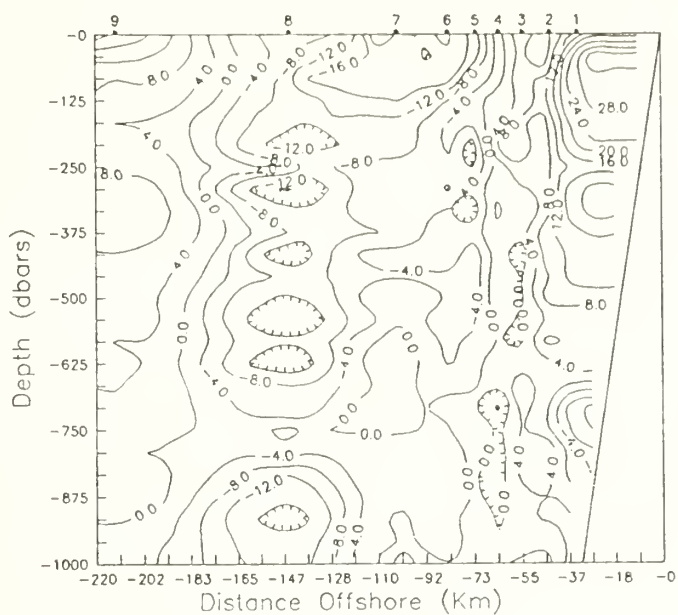
Figure 19.   Pegasus V Velocities. Top first run. Bottom second run

and tides may affect the undercurrent at surface. This may be related to the NW wind
because the winds become stronger during the time interval from the first measurement

of the Sites C1 and C2 to the second. It is expected such a wind will cause an offshore increase of width of the northward flowing undercurrent. This increase is due to the Coriolis force which deflects the water to the right. The picture of the southward flowing California Current looks almost the same for the two runs giving the core at 110 km offshore.

The important conclusion is that in both cases the general picture is the same, presenting strong the northward flowing California Undercurrent and the in-shore branch of the southward flowing California Current.

Table 8.   SUMMARY OF THE PEGASUS RESULTS

Flow charac-teristics	V1 (1st run)	V2 (2nd run)	V (Aver-age)	U1 (1st run)	U2 (2nd run)	U (Av-erage)
Width (km)	< 63	< 84 at sfc and < 54 at 50 dbars	< 75	< 62	< 82 at sfc and < 46 at 50 dbars	< 52
Depth (dbars)	650	700	650	700	700	700
Direction	North	North	North	West	West	West
Speed (cm/sec)	32	32	32	16	16	16
Core's dis-tance (km)	< 33	< 33	< 33	< 33	< 33	< 33
Core's depth (dbars)	50	50	50	sfc	sfc	sfc
Width (km)	63 - 174	84 - 193	75 - 180	62 - 220	82 - 220	52 - 220
Depth (dbars)	300	300	300	600	400	600
Direction	South	South	South	East	East	East
Speed (cm/sec)	24	28	24	20	20	20
Core's dis-tance (km)	105	110	110	180	150	150
Core's depth (dbars)	sfc	sfc	sfc	70	100	100
Width (km)	> 174	> 193	> 180			
Depth (dbars)	800	1000	1000			
Direction	North	North	North			
Speed (cm/sec)	< 8	< 8	< 8			
Core's dis-tance (km)	> 210	> 210	> 210			
Core's depth (dbars)	sfc	70	sfc			

(2) U Velocities

As was done for the V velocities, I tried to examine the relationship of the U velocity for each station for the first and the second run looking at the mean and the standard deviation horizontally for every 20 bins. The standard deviation values show that the greatest variation of the U velocities between first and second run occurs close to the shore (Sites C1, C2) and mainly in the upper layers. The main reasons which cause these variations, it is estimated, are the same as for V velocity (tidal waves, wind, navigation errors, etc). Taking into mind that wind can cause remarkable increase or decrease of the U velocities and checking how the wind velocity changes from the first to second run we expect such great values of standard deviation.

The conclusion from the study of the standard deviations of the U and V velocities is that the greatest variations occur close to the shore, and mainly in the upper layers. This leads to the assumption that an external factor mainly causes these variations. This external factor should be the wind, which causes the inertial motion and affects the current's velocities or tides etc. This has to be investigated in the future with current meter data to form a better picture of the short term variability.

Figure 20 gives the average cross section of U velocity including the results of all these factors which cause the velocity variations. In this picture are observed three flow regimes. The first one, close to the shore, is a westward surface current which starts from the surface and extends to a depth 750 dbars. This flow is stronger close to the shore and weakens as it extends offshore about 70 km. The maximum speed of 20 cm/sec is on the surface. The second regime is an eastward/landward flow starting from 70 km offshore and extending all the way offshore to Sites C9. The maximum speed of this is 20 cm/sec observed on a depth 160 dbars, but as the depth increases the current weakens. Between Sites C8 and C9 this flow is extended to a depth of 650 dbars but between Sites C8 and C6 the inshore current extends all the way down to the bottom.

Finally there is a weak offshore flow between Stations C8 and C9 which starts at a depth 650 dbars and extends downward to the bottom. This weak offshore flow doesn't exceed the 4 cm/sec and in most of the places is approximately zero. As it is shown in Figure 25 we see two centers of the flow. One center for the offshore flow and one for the inshore flow. The center of the offshore flow is located close to the shore at a distance 30 km from the shore and depth 30 dbars. The center of inshore flow is located at a distance 155 km offshore and at a depth 165 dbars.
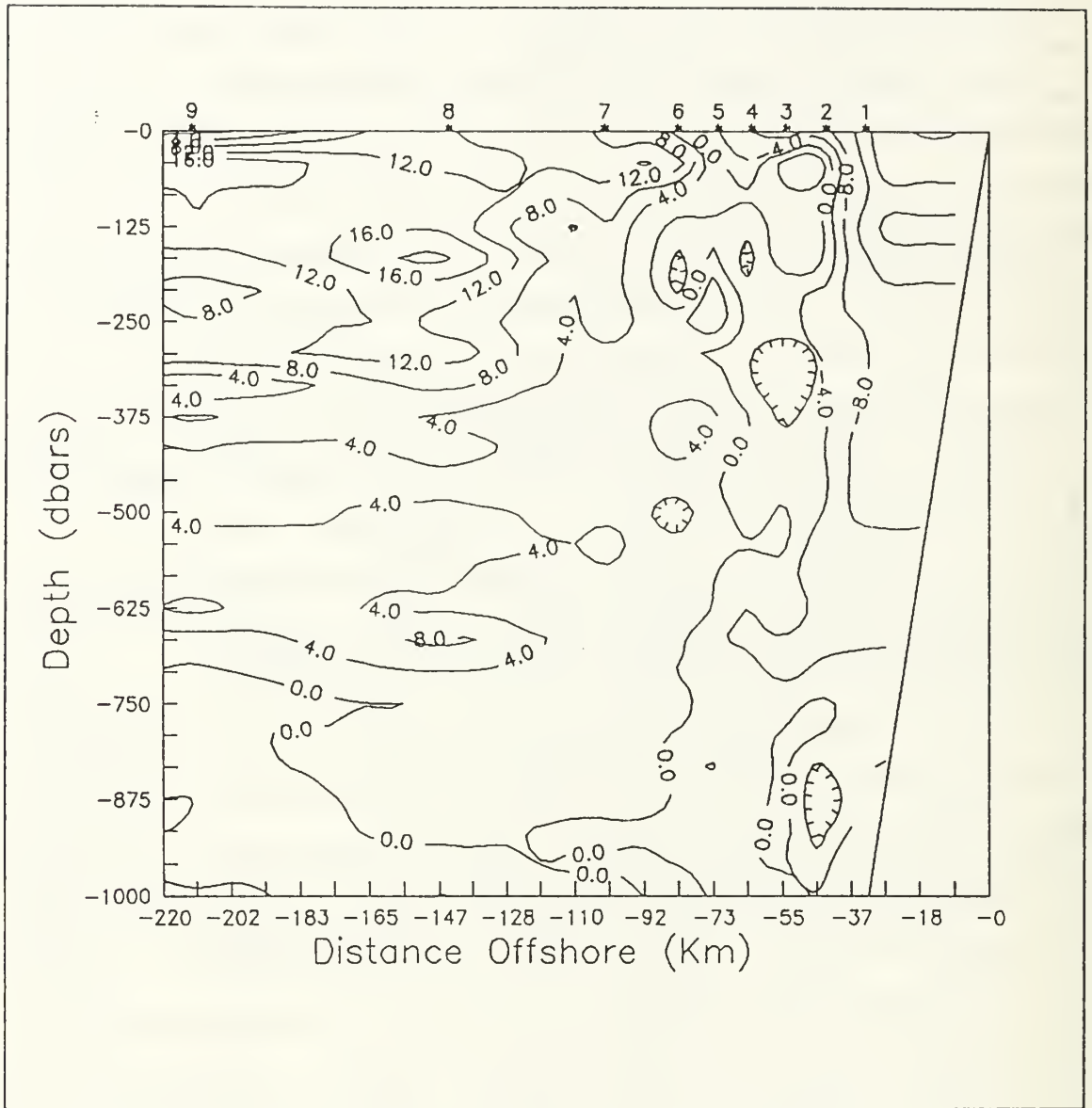
Figure 20.   Pegasus U Velocities. Average velocities of the runs

To compare the U velocities of the first and second run, a description of the U velocities cross section follows for the two runs (Figure 21). The important conclusion from this description is that the picture of the two runs is about the same. The effects of an external force (most possible the wind) are shown clearly where strongest westward velocities occur at the second run due to the increase of the wind force during the time period between the two runs.
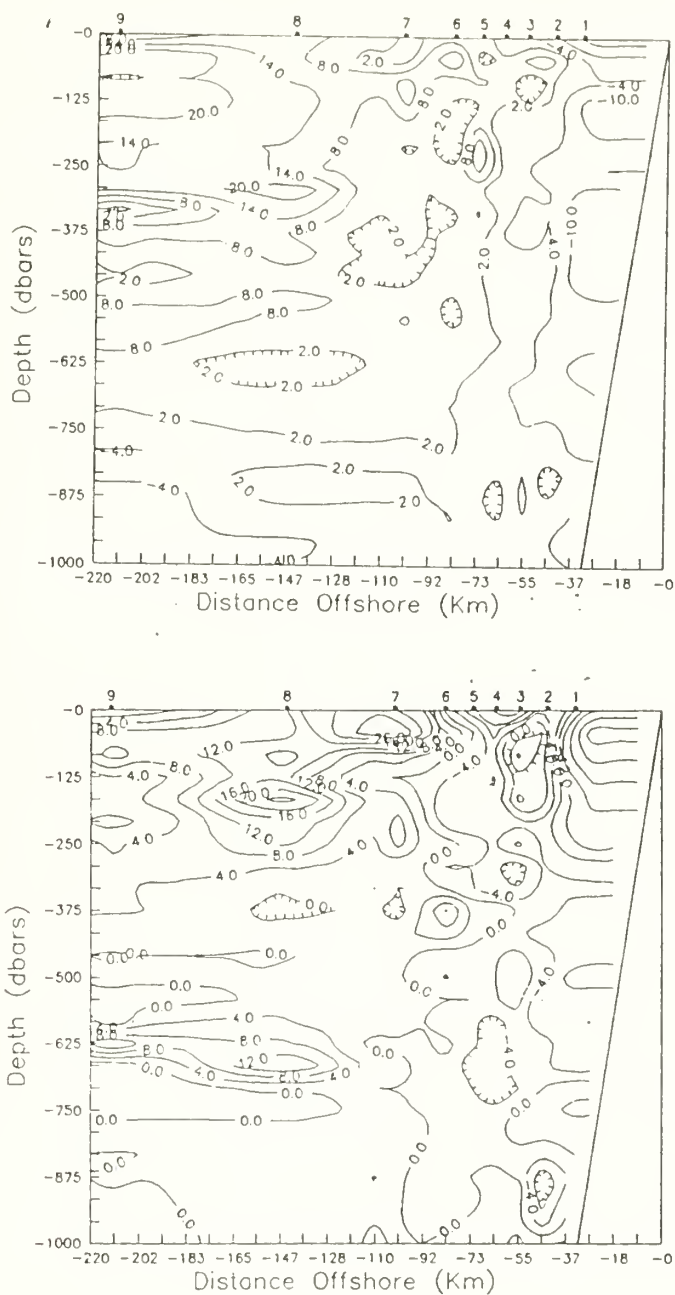
Figure 21.   Pegasus U Velocities. Top first run. Bottom second run

        The first run (the drop numbers given above) shows westward flow
close to the shore until the Site C3. This westward flow extends downward to 700 dbars

below of which becomes eastward. Offshore from Site C3 eastward velocities are shown which become stronger as the distance offshore increases. Largest velocities occur in the first 300 dbars. At greater depths these velocities become smaller than 2 cm/sec. At distances 180 km offshore and below 1000 dbars weak westward flow occurs. As the depth increases this weak westward flow approaches to zero.

The second run gives about the same picture as the first run. Close to the shore westward velocities occur, which at the surface are stronger and reach to a distance of 82 km offshore. As the depth increases the speed of the westward flow becomes smaller and below 1500 dbars depth no westward flow occurs. Offshore from Station C6 a stronger eastward flow occurs. The strongest velocities occur close to the surface and reach to a value of 16 cm/sec. As the depth increases the flow weakens and at the depth of 500 dbars no eastward motion is shown. Deeper than 500 dbars (600 to 800 dbars) an eastward flowing core is shown which disappears after 800 dbars. In greater depths no water motion is shown.

(3) Pegasus plan view

Figure 22 presents the Pegasus determined velocity vectors at three depths (10, 110 and 210 dbars). The Undercurrent flows northward following the local trend of the isobaths with a larger offshore component at the surface. The surface flow may be influenced by the local upwelling at Point Sur. The flow reversal seen at Site C6 marks the transition from the Undercurrent to the California Current. Farther offshore at C9 the meander tendency of the California Current is observable by the velocity vectors.

c. ADCP Velocities

To get the ADCP U and V velocity profiles, I used the time that Pegasus instrument was dropped into the water and the time that the Pegasus surfaced. On the basis of these times and using 30 minutes time intervals (15 minutes before and 15 minutes after) I plotted the U and V velocities for the first and the second run as defined for Pegasus. This allows a good comparison of ADCP and Pegasus data.

(1) V Velocities

The average ADCP V velocities of the two runs show:

- Close to the shore to a distance 65 km offshore, poleward flow whose the maximum speed is 32 cm/sec. The core of this poleward flow is at a distance 32 km offshore and the depth 40 dbars. The greatest depth of this poleward flow is 340 m.

- From 65 km offshore to 170 km offshore equatoward flow occurs. The core of this flow is at 110 km offshore and the at a depth 30 dbars. The highest speed is 28 cm/sec and occurs close to the surface. In general the speed of this current is
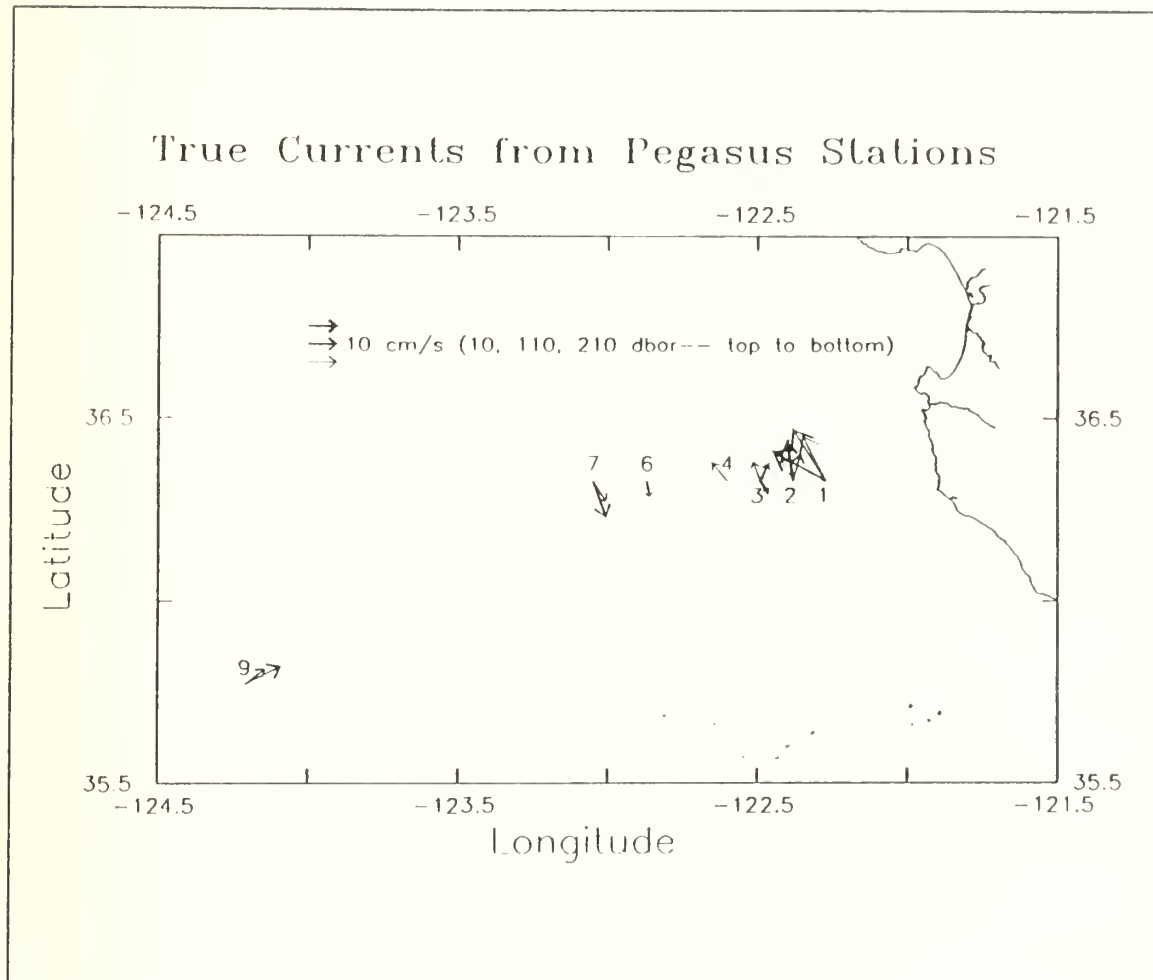
44

Figure 22.   Pegasus true velocities

smaller than the speed of the poleward flow close to the shore. Further offshore
from 170 km the flow is again northward but quite smaller than the inshore regions.

        To examine the relationship (similarities/differences) between the two
runs a description of them follows which shows clearly that both of them give the same
results with the exceptions that in the second run:

- The northward flowing California Undercurrent extends further offshore than in
  the first and

- At distances greater than 170 km there was no northward flowing current on the
  surface.

Both exceptions lead to the assumption that phenomena like inertial motion, wind or
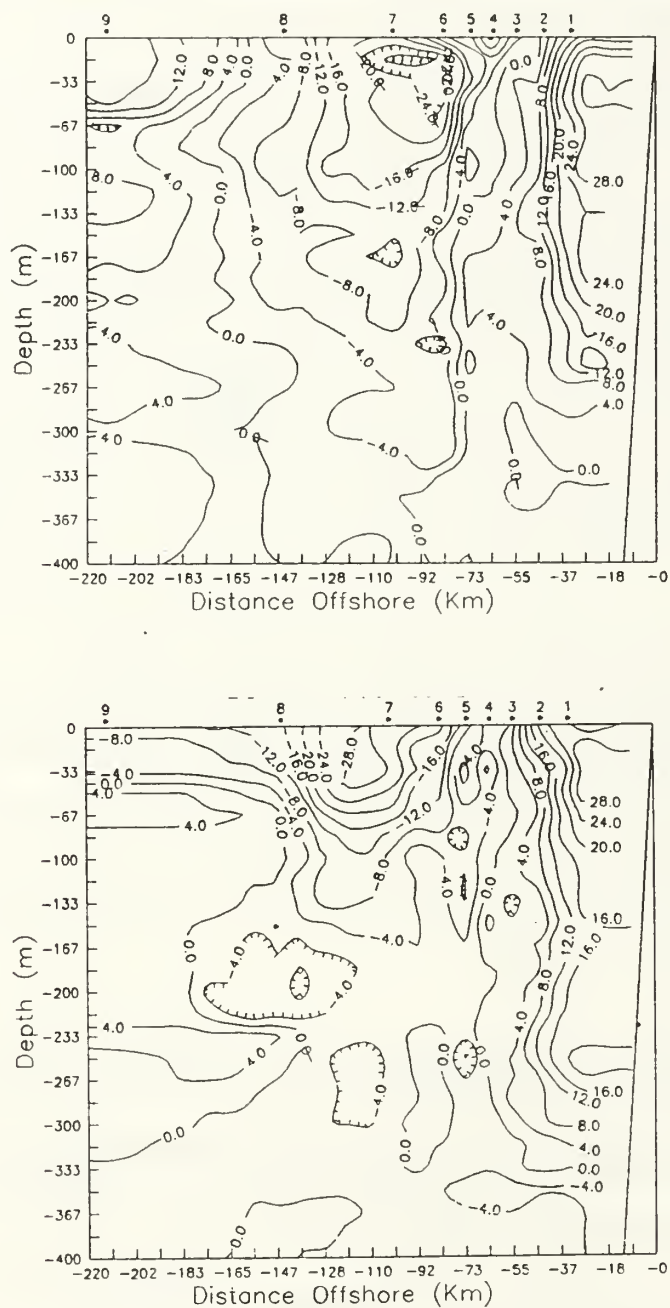tidal waves affect the currents in the area.

Figure 23.   ADCP V Velocities. Top first run. Bottom second run

ADCP V velocities for the first run show strong northward flow close to the shore until a distanse 40 km offshore. This strong northward flow occurs in all the

range of the depth (400 m) with almost the same strength. From 40 to 170 km southward flow occurs. This flow is shown stronger in the upper layers and weakens as the depth increases. The greatest velocity is 28 cm/sec at a depth of 30 dbars. Last, offshore from 170 km northward flow is again shown with stronger velocities at surface. These extend to whole the range of the depth 400 dbars.

V velocities of the second run present quite the same picture as in the previous case. The only difference is that in the upper 30 dbars and offshore from 170 km, we don't get the northward weak velocities as in the previous case, but these start after this depth.

Comparing the ADCP V velocities plots with the Pegasus V velocities, we see excellent correspondence. Northward flow close to the shore in the upper 700 dbars (this depth cannot be seen in the ADCP plots) with greatest speed 36 cm/sec, and southward weaker beyond 42 km offshore at surface and 60 km at depth. Offshore from 170 km northward weak flow again occurs.

(2) U Velocities

The average U velocities show:

- Close to the shore a westward flow, with the velocity greater at the surface and decreasing as the depth increases. The westward flow is shown in all the range of the depth (400 m) and it is stronger closer to the shore. The offshore limit of this flow is at 35 km from the shore.

- At 35 km offshore an eastward flow whose the velocity increases as the distance offshore increases. At 115 km offshore the eastward flow reaches its maximum speed on the surface. Further offshore the surface speed decreases.

- At 175 km offshore, a westward flow appears. This flow occurs only at surface because below 60 dbars an eastward and relatively strong core flows which extends downward to 400

ADCP U velocities for the first and second run give the same picture in the area.

- Westward flow at the surface close to the shore, which shows in a distinct way the proccess of the upwelling and

- Eastward flow at distances greater than 45 km from the shore to 165 km.

- Weak westward flow again after 165 km offshore.

Comparing this with the results from Pegasus measurements we get an excellent correspondence. Table 9 gives an integrated picture of U and V velocities in the area measured by the ADCP.
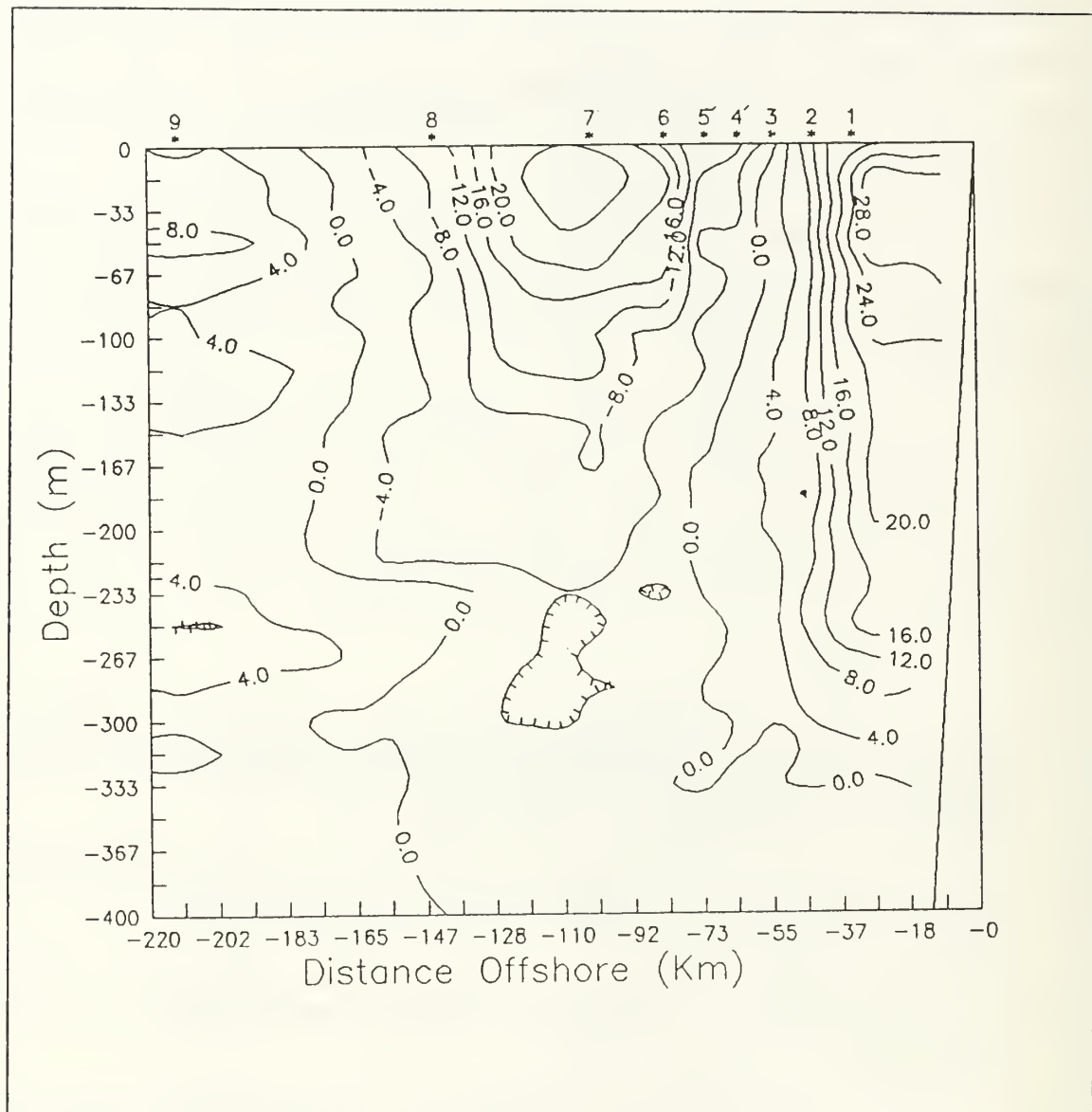
Figure 24.   ADCP V Velocities. Average velocities of the runs

10.   CUC Transport

The CUC transport was calculated by first dividing the whole cross section of the CUC in smaller sections and then was taking into account the most appropriate speed for the section. The result is that the Undercurrent's northward transport during June 1990 was 2.9 Sv. Relating this value with previous results we see that the CUC for June 1990 shows a medium size transport.
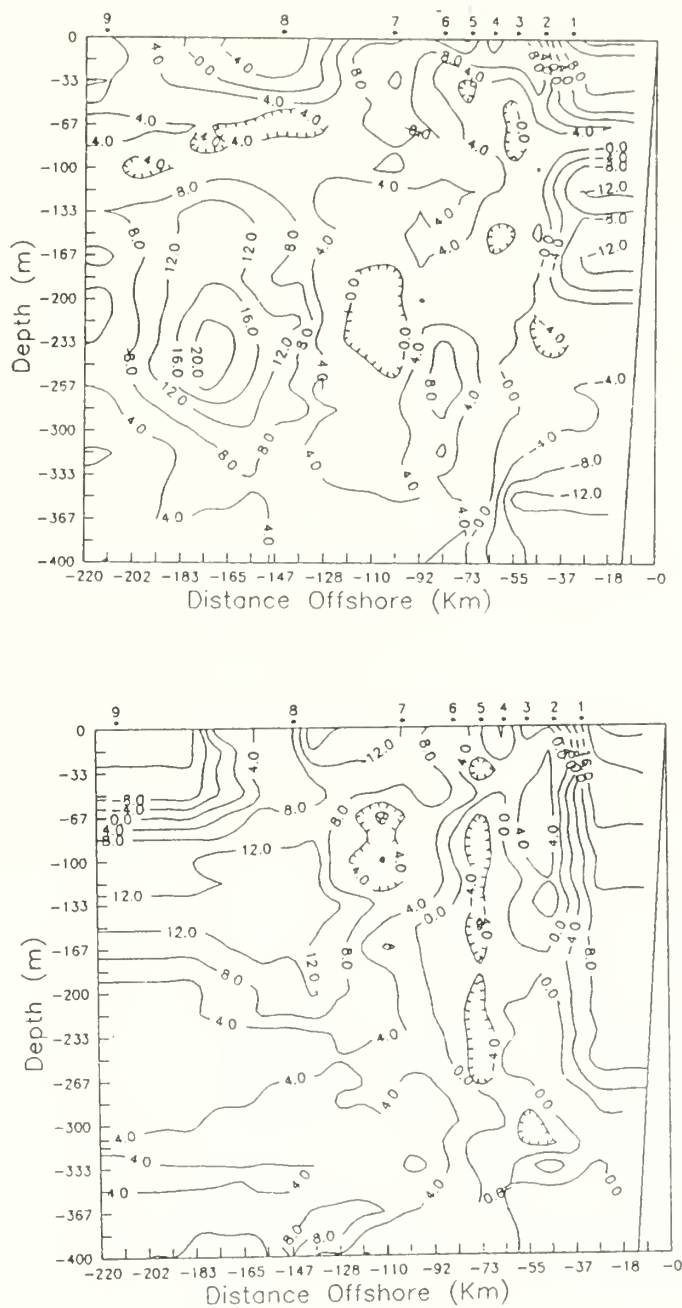
48

Figure 25.   ADCP U Velocities. Top first run. Bottom second run
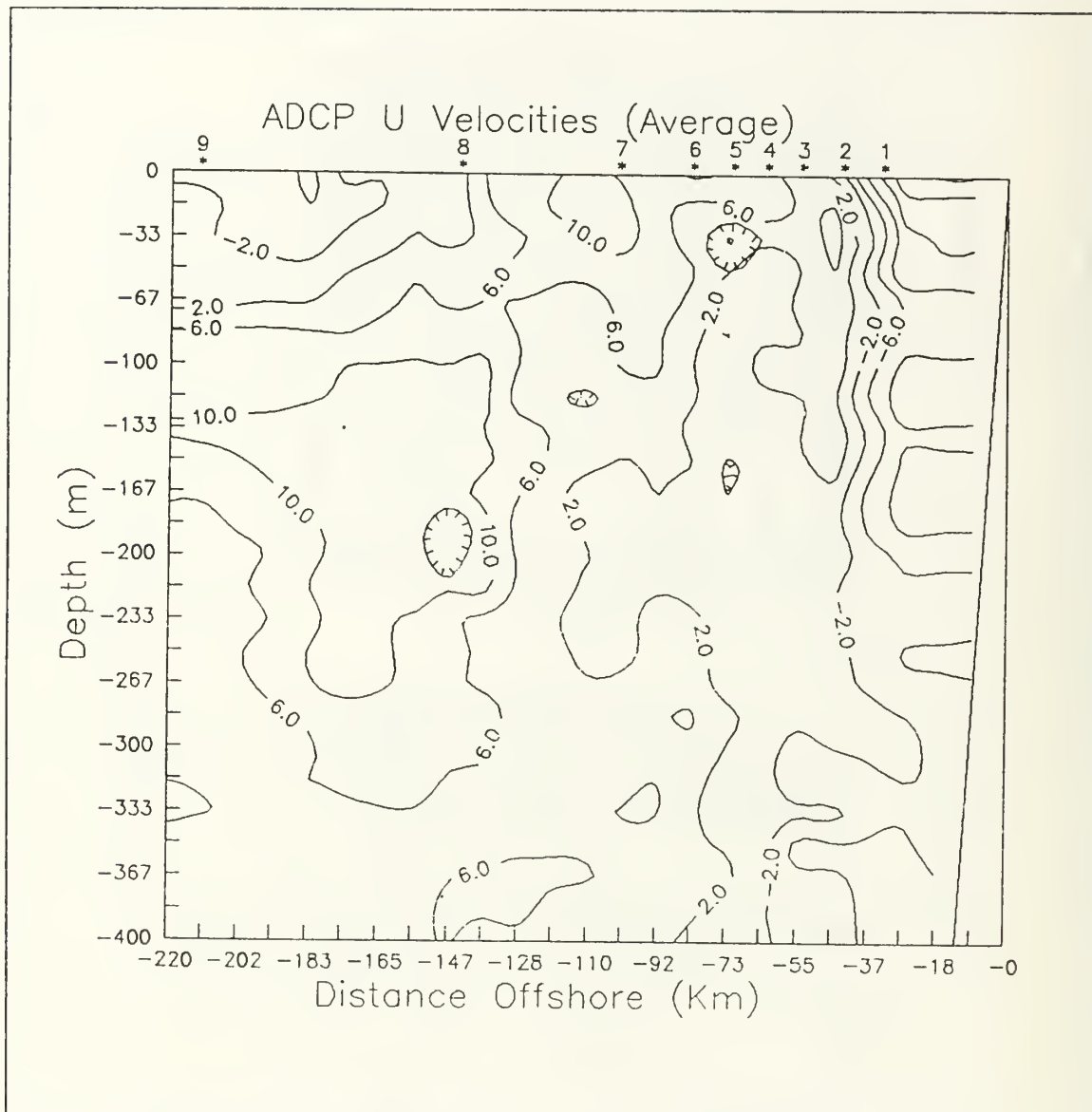
11.   AVHRR Imagery

Figure 26.   ADCP U Velocities. Average velocities of the runs

The Advanced Very High Resolution Radiometer (AVHRR/2) instruments, carried on the TIROS-N/NOAA series of polar orbiting satellites, are used to obtain Sea Surface Temperature (SST) images for the study region. The AVHRR/2 instruments measure emitted radiation in five wavelength bands, visible (0.6-0.7 μ m), near infrared (0.7-1.1 μ m), and thermal infrared (3.5-3.9 μ m, 10.5-11.5 μ m). Using the thermal IR bands enables estimation of the sea surface temperature, correcting for atmospheric

50

Figure 27.   AVHRR IR Image

contamination (McClain et al. 1985). The satellite data were first calibrated and navigated to Earth coordinates. When possible, temperature was computed pixel by pixel, followed by land masking and cloud detection.

Data for 20 June 1990 are given in Figure 27. Starting from offshore to the southwest the ocean is obscurred by a warm cloud which extends to the northeast halfway between the Stations 19 and 20. The warm temperature of the cloud indicates that this is very low. The rest of the image appears clear over the ocean. Four distinct cold water sources are observed north of 35 ° N. One at Point Lopez, second at Point Sur, third at Pt Ano Nuevo (north of Santa Cruz) and the last at Pt Reyes. Plumes of cold water (light grey) extend away from these sites. The Pt Sur transection at 36°20′ N ap-

Table 9.   SUMMARY OF THE ADCP RESULTS

Flow charac-teristics	V1 (1st run)	V2 (2nd run)	V (Aver-age)	U1 (1st run)	U2 (2nd run)	U (Av-erage)
Width (km)	< 55	< 55	< 55	< 45	< 45	< 42
Depth (dbars)	400	330	350	400	30	400
Direction	North	North	North	West	West	West
Speed (cm/sec)	32	28	28	16	24	22
Core's dis-tance (km)	< 33	< 33	< 33	< 33	< 33	< 33
Core's depth (dbars)	50	50	50	sfc	sfc	sfc
Width (km)	55 - 155	> 55	55 - 180	45 - 165 (sfc) and 45 - 220 (below 30 dbars)	45 - 165	40 - 150 (sfc) and to 220 be-low 30 dbars
Depth (dbars)	400	160	220	400	400	400
Direction	South	South	South	East	East	East
Speed (cm/sec)	28	28	24	20	16	14
Core's dis-tance (km)	100	115	110	175	155	160
Core's depth (dbars)	30	30	30	240	150	180
Width (km)	> 170	> 165	> 180	> 135	> 165	> 150
Depth (dbars)	400	30 - 230	400	sfc - 30	sfc - 60	sfc - 50
Direction	North	North	North	West	West	West
Speed (cm/sec)	16	4	8	4	12	8
Core's dis-tance (km)	210	> 210	> 210	155	> 210	180
Core's depth (dbars)	sfc	50	30	sfc	sfc	sfc

parently bisects two of these plumes as indicated by the colder surface water from Stations 1-5 and 10-15. Offshore of Station 15 warm water (dark grey) appears again whose the temperature increases as the distance offshore increases.

The satellite image related with the velocities and phenomena discussed previously suggest that the cold water close to the shore comes from Pt Sur. Offshore the water is strongly affected by a cold plume derived from one of the northern sites.

According to the velocity descriptions off Point Sur, close to the shore warm poleward flow extends to a distance 75 km offshore with the core at 33 km. In addition westward flow takes place strongly affected by the wind stress and amplifying the upwelling in the area. The above leads to the conclusion that close to the shore the waters coming up are mixed with the warm northward flowing current and lie in the area extending westward. The strong upwelling close to the shore extends offshore to Station 5. Between Stations 5 and 10 there is a tongue of warm water separating plumes of colder upwelled water.

Offshore from Station 10, as it was mentioned earlier, cold waters again appear on the surface. Recalling the velocities section described before, offshore from Station 10 the California Current appears on the surface flowing southward. This gives the idea that waters coming from the north are in the area. Figure 27 shows clearly the phenomenon. The cold waters appearing in the area are the waters of the two northern upwelling centers. These waters came up from a depth and then because of upwelling favorable winds were drawn southward and affect the area between Stations 10 and 15.

Further offshore from Station 15 warm waters cover the all area becoming warmer as the distance offshore increases. Here the upwelling centers do not affect the sea surface temperature.

Stations 20 to 22 are under the clouds and the sea surface temperature cannot be detected.

B. DISCUSSION

The poleward undercurrent over and along the continental slope has been observed at several latitudes between Baja, California and Vancouver Island. According to Tibby (1941) and Reid (1958) indirect evidence of this flow is clearly visible in the large-scale temperature-salinity characteristics of coastal waters as northward-tending tongues of relatively warm, saline water. More detailed studies of particular regions also show a concentration of waters of more southerly origins along the continental margin (e.g., Wickham, 1975; Reed and Halpern, 1976). Chelton (1984), from an analysis of CalCOFI sections off Point Sur describes that the undercurrent off Point Sur, is confined to the continental slope region within 75-100 km of the coast. This nearshore poleward flow at depth is absent March-May. It first appears in June-July and is present through February. The poleward flow extends all the way to the surface from October through February with maximum poleward velocity at surface in December (14 cm/sec). During the remainder of the year the maximum poleward flow is below the surface. According

to the same study, the undercurrent off Point Sur was never observed in June and only weak poleward flow has ever been observed in July. The diagrams exhibited in his report giving the seasonal time series of alongshore geostrophic velocity at the surface and 150 dbars with respect to LNM 500 dbars show southward flow at surface and zero velocities at 150 dbars during June.

Data from June 1990 clearly show that the colder waters are closer to the shore and the warmer offshore. Salinity cross section shows that the more saline water is close to the shore. The background knowledge about the physical phenomena in the area during this period gives the information that this period is the upwelling period and low temperature and high salinity waters are expected in the area. Temperature and salinity profiles (Figures 5, 7) give the picture that water masses of more southerly origins flow along the continental margin. This can be concluded by the fact that a core of relatively warm and saline water flows northward surrounded by colder upwelled saline water. The offshore limit of this northward flowing core is located between 60 to 70 km offshore and vertically extends from surface to 700 dbars. As the geostrophic velocities and V velocities of the Pegasus and ADCP data show, on the surface this northward flowing current is narrower but at depth of 200 to 300 dbars gets its maximum width of 60 to 70 km. These results agree with the countercurrent described by Sverdrup and Fleming (1941). In my case the countercurrent is observed at the surface too. Refering to the more recent descriptions of the undercurrent/countercurrent at Point Sur by Chelton (1984), June 1990 data show a much different picture. Chelton determined that the undercurrent wasn't observed in the years 1950 to 1979. The strong Undercurrent observed close to the shore in June 1990 suggests that Chelton may not have had stations sufficiently close to shore. The lack of an Undercurrent may have been due to the data distribution rather than real variability.

The bend of the isotherms, isohalines and isopycnals upwards toward shore clearly shows the upwelling in the upper 100 dbars. Comparison of AVHRR and temperature section demonstrates that upwelling plumes are shallow features. This is in phase with the Sverdrup assumption that the upwelling water rises from moderate depths only, probably less than 200 m (Sverdrup and Fleming, 1941) and the phenomenon represents only an overturning of the upper layers. Closer examination of U velocities measured by Pegasus and ADCP can give an idea of the upwelling in the area, which happens at a distance from the shore. In all the cases, far offshore a relatively strong eastward flowing core is observed at depths 100 to 150 dbars. This core shallows and weakens closer to the shore, giving the idea of the upwelling offshore.

T/S characteristics clearly give the expected water masses in the area. As was described earlier, the equatorial water masses flowing northward in the area affects the Subarctic North Pacific water mass flowing southward and close to the shore creates the bend in the T/S characteristics. In the upper layers (surface to 150 dbars) we can distinguish two different water masses. One of the them is for the stations close to the shore (Stations 1 to 10) and the other far offshore. T/S characteristics of the Stations 10 to 15 (in the upper layers) lie between the T/S characteristics of the two masses. The first one (between Stations 1 and 10) has high salinity and low temperature, the second has low salinity and higher temperature. This construction clearly gives the picture of the Equatorial Water mass close to the shore affected by the upwelling and the less saline Subarctic North Pacific water mass offshore. The product from the contribution of the two water masses is shown clearly just below the 150 dbars where the bend of the characteristics is shown. Another important point is at the depth of 300 to 700 dbars where stations offshore from station 14 present T/S characteristics different than the other stations. This gives an idea that at this depth the northward flowing undercurrent, which carries Equatorial waters, is restricted in the area close to the shore. Further offshore the Subarctic North Pacific water mass dominates.

The Level of No Motion determination still remains uncertain because there is no method which guarantees this. Some of the most acceptable methods were applied and the result was that the most representative LNM was at 700 dbars. I believe that close to the shore the LNM is somewhat shallower. Offshore it becomes greater, but this has to be investigated by the current meters. An indication for the LNM is given by the salinity differences between the stations in pairs. These show that with a depth they tend to close to zero, giving an idea that below this depth the water motion in the area is almost zero and the water is almost homogenous. The depths where the salinity differences close to zero varies offshore. Close to the shore the zero difference in salinity between the stations is observed at a depth of 400 dbars, further offshore the depth increases reaching to 1000 dbars. Of course the depths where the differences in salinity close to zero cannot be accepted as the depth of the LNM because horizontal and vertical diffusion factors are taken into account, but still there is a good indication of the level where the motion is very small. Density differences between the stations give a better picture of the LNM depth. The reason for this was described analyticaly in the LNM section. The depth where the density differences close to zero and the range of depth where the dynamic height differences show constancy agree giving the results mentioned before.

The geostrophic, Pegasus and ADCP velocities give an integrated picture of how the coastal jet, California Undercurrent and California Current look in June 1990. The California Undercurrent is the most important characteristic in the area, and for June 1990 presents features much different than those described by Chelton (1984) using averaged data for many years. According to the data of June 1990, the California Undercurrent off Point Sur is shown to occupy the area from Station 2 to Station 9 at the surface. Deeper (100 to 300 dbars) the Undercurrent becomes wider reaching to Station 12. Deeper than 300 dbars it becomes narrower and extends to the depth of 700 dbars. The maximum northward velocity of this is shown at distance 25 km from the shore, depth 100 to 150 dbars and it is 36 cm/sec. The data give a different picture of the Undercurrent than this described by Sverdrup et al. in "The Oceans" (1960). According to them, the Undercurrent is a northward flow at depth 200 m.

Relating the results for the Undercurrent from data of June 1990 with those from the previous seven cruises analysed by students of the Naval Postgraduate School, June 1990 gives about the same picture. Tisch (1990), studying the seasonal variability of the geostrophic velocity and water mass structure Off Point Sur for the seven previous cruises, said that the Undercurrent core is located within 42 km offshore and in depths between 70 to 460 dbars on all cruises. The CUC was present at the surface in February 1989 and November 1989 and subsurface throughout the remainder of the year. In 1988 poleward flow at surface was only seen in November and inshore of Station 3. The warmest and saltiest waters were found at the depth of the CUC. Strong surface poleward flow was observed in May 1989 inshore of Station 5 as result of warmer fresher water found further offshore. In August of 1988 and July of 1989 strong poleward surface flow was also observed due to significant relaxation of equatorward winds which occurred 2 days prior to the July cruise and during the August cruise.

The above observations related with the results of June 1990 lead to the conclusion that the California Undercurrent exists close to the shore throughout of the year within 42 km offshore. The location of the core exhibits great variations in depth but generally small in distance offshore (almost all the values were between 15 and 28 km offshore). The possibility is not excluded that the undercurrent be observed on the surface as in February 1989, November 1989 and June 1990.

IV. CONCLUSIONS AND RECOMMENDATIONS

A. CONCLUSIONS

The purpose of this study was to characterize the dynamic structure, transport, and water mass character of the California Undercurrent and California Current using data from CTD, Pegasus, ADCP and AVHRR.

The California Undercurrent during June 1990, is remarkably strong and surfaced in contrast with the analysis of CalCOFI data by Chelton (1984). While some of this variability is real due to fluctuations of the Undercurrent, earlier observations did not have the spatial resolution to always resolve the flow. The maximum speed at the core is 36 cm/sec, located 33 km offshore. It is shown to be strongly affected by the wind force, at least in the upper 50 dbars. One day duration of upwelling favorable wind force or one day compensation may be enough to remarkably change dimensions of the Undercurrent at surface. It is estimated that a greater than one day duration of the wind's compensation can cause the disappearance of the California Undercurrent from the surface and the area until the coast be covered by the Davidson current.

The California Undercurrent during June 1990 is restricted in the upper 700 dbar and mixes equatorial type waters with the Subarctic North Pacific water in the area. This is shown very distinctively in the T/S diagrams. The CUC transport is estimated to be 2.9 Sv.

The California Current is shown to be shallow (less than 300 dbars) and with smaller velocity (28 cm/sec) than the California Undercurrent. The landward limit of the surface flow is located at Station 9 and presents a surface core at distance of 110 km from the shore. It carries Subarctic North Pacific water which is distinguished by low temperature and salinity. As the T/S diagram illustrates, the landward limit of the CC is strongly affected by the characteristics of the Undercurrent, mainly below 150 dbars. On the surface the effects of the Undercurrent are not so strong but still the surface characteristics of some of the stations are between the two distinct water masses.

The upwelling is shown reaching to a depth of 100 dbars and affecting mainly the waters landward of Station 5 (22 km from the shore). This phenomenon was driven by the upwelling favorable NW winds.

The southward flowing coastal jet is present the data of June 1990. Landward from Station 2 a southward, narrow and shallow current is shown on the surface, having maximum velocity 10 cm/sec.

A detailed analysis of all data leads to the conclusion that 700 dbars is a more accurate estimate of the LNM than either 500 or 1000 dbar.

B. RECOMMENDATIONS

Data of June 1990 give a picture of the currents in the area which are amplified or compensated by such local phenomena as upwelling, tidal waves, inertial motion, and winds. Using data from CTD, Pegasus, ADCP and AVHRR concentrated on a line it is almost impossible to express an opinion for the size of contribution of the local phenomena on the currents in the area. I estimate that to form a statistical correlation of how much the local phenomena contribute on the currents, the results of this study have to be compared with data from other sources, as for example from current meters and a sampling array covering an area rather than just a line.

REFERENCES

- Berryman, P. Study of Currents Along the Point Sur Transect in February 1989. Master's Thesis, Naval Postgraduate School, Monterey, California, September 1989.

- Blanton, J. and J.G. Pattullo (1970) The Subsurface Boundary Between Subarctic Pacific Water and Pacific Equatorial Water in the Transition Zone Off Southern California. Limnology and Oceanography. 15(4), 606-614.

- Brink, K.H. The Near-Surface Dynamics of Coastal Upwelling, Prog Oceanog. 1983. Vol. 12, pp. 223-257.

- Chelton, DB., Seasonal variability of Alongshore Geostrophic Velocity Off Central California, J. Geophys. Res. 89,3473-3486,1984.

- Chelton, D.B., R.L. Bernstein, A.W. Bratcovich, and P.M. Kosro, The Central California Circulation Study. EOS Transactions, American Geophysical Union Vol 68 No. 1 January 6, 1987.

- Chelton, D.B., R.L. Bernstein, A.W. Bratcovich, and P.M. Kosro, Poleward Flow off California During the Spring and Summer. Journal of Geophysical Research, Vol 93, No C9, pp 10604-10620, September 15, 1988.

- Collins, C.A., C.N.K. Mooers, M.R. Stevenson, R.L. Smith, and J.G. Pattulo, Direct Current Measurements in the Frontal Zone of a Coastal Upwelling Region, J. Oceanogr. Soc. J., 24, 31-42, 1968.

- Defant, A., vol I,II Physical Oceanography, Pergamon Press, 1961.

- Flamment, P., submitted 1986: A note On Seawater Spicinness and Diffusive Stability. Deep Sea Res.

- Fofonoff, N.P. Physical Properties of Seawater, J. Geophys. Res. 90 3332-3342, 1985.

- Fomin, L.M., The Dynamic Method in Oceanography, Elsevier, 1964.

- Gross, M.G., B.A. Morse and C.A. Barnes (1969) Movement of Near-Bottom Waters on the Continental Shelf Off Northwest United States. Journal of Geophysical Research, 74, 7044-7047.

- Halpern, D., R.L. Smith and R.K. Reed (1978) On the California Undercurrent Over the Continental Slope Off Oregon. Journal of Geophysical Research, 83(C3), 1366-1372.

- Hickey, B.M. The California Current System-Hypothesis and Facts, Progr. Oceanogr.,Vol 8, pp.191-279, 1979.

- Huyer, A. Coastal Upwelling in the California Current System, Prog. Oceanogr., Vol 12, pp.259-284, 1983.

- Huyer, A., R.D. Pillsbury and R.L. Smith (1975a) Seasonal Variation of the Alongshore Velocity Field Over the Continental Shelf Off Oregon. Limnology and Oceanography, 20, 90-95.

- Huyer, A., R.L. Smith, and E.J.C. Sobey (1978) Seasonal Differences in Low-Frequency Current Fluctuations Over the Oregon Continental Shelf. Journal of Geophysical Research, 83, 5077-5089.

- King, C.H. A Comparison of Pegasus and Combined CTD ADCP Current Profiles off the California Coast, Master's Thesis. Naval Postgraduate School, Monterey, California, March 1989.

- Kosro, P.M., Shipboard Acoustic Doppler Current Profiling During the Coastal Ocean Dynamics Experiment, Ph.D.Dissertation, SIO Ref 85-8, Scripps Institution of Oceanography, 1985.

- McClain, E.P., W.G. Pichel and C.C. Walton. 1985 Comparative performance of AVHRR-based multichannel sea surface temperatures. J. Geophys. Res. 90:11,587-11,601.

- Mooers, C.N.K., C.A. Collins, and R.L. Smith. The Dynamic Structure of the Frontal Zone in the Coastal Upwelling Region Off Oregon, J. Phys. Oceanogr., 6, 3-21, 1976.

- Moschovos, I.S. Compare at Sea Position Using Mini-Ranger, LORAN C (INTERNAV) in the Context of Measuring Current Velocity with a Shipboard ADCP, Master's Thesis Naval Postgraduate School, Monterey, California, December 1989.

- Pavlova, Y.V. (1966) Seasonal Variations of the California Current. Oceanology, 6, 806-814.

- RD Instruments, Acoustic Doppler Current Profilers. Principles of Operation. A Practical Primer, San Diego California 1989.

- Reece, R.H.. An analysis of Hydrographic Data Collected off Point Sur, Callifornia in November 1988, Master's Thesis. Naval Postgraduate School, Monterey, California, September 1989.

- Reed, R.K. and D. Halpern (1976) Observation of the California Undercurrent off Washington and Vancouver Island. Limnology and Oceanography, 21, 389-398.

- Reid, J.L., Physical Oceanography, 1947-1987, CalCOFI Reports XXIX, 42-65, October 1988.

- Reid, J.L., Jr. and G.I. Roden and J.G. Wyllie (1958) Studies of the California Cooperative Oceanic Fisheries Investigations Progress Report, 7-1-56 to 1-1-58, Marine Resources Committee, California Department of Fish and Game, Sacramento, California, 27-56.

- Shepard, F.P. Submarine Topography Off the California Coast, Canyons and Tectonic Interpretation, Geological Society of America Special Papers Number 31, May 28, 1941.

- Shepard, F.P., N.F. Marshall, P.A. McLoughlin, G.G. Sullivan. Currents in Submarine Canyons and Other Seavalleys. The American Association of Petroleum Geologists. Tulsa, Oklahoma, U.S.A. 1979.

- Spain, P.F., D.L. Dorson, and H.T. Rossby, PEGASUS, a Simple Acoustically Tracked, Velocity Profiler, Deep Sea Res., 1553-1567, 1981.

- Sverdrup, H.U., and R.H. Fleming. 1941. The Waters Off the Coast of Southern California, March to July, 1937. Scripps Inst. Oceanogr., Bull., v. 4, no. 10, p.261-378, 1941.

- Sverdrup, H.U., Johnson M.W. and Fleming R.H. The Oceans, Prentice-Hall, INC November 1964.

- Tchernia, T. Descriptive Regional Oceanography, Pergamon Press 1980.

- Tibby, R.B., 1941. The Water Masses Off the West Coast of North America. Jour. Marine Research, v. 4, p. 112-121, 1941.

- Tisch, T.D. Seasonal Variability of the Geostrophic Velocity and Water Mass Structure Off Point Sur, California. Master's Thesis, Naval Postgraduate School, Monterey, California, September 1990.

- Wickham, J.B. (1975) Observations of the California Countercurrent. Journal of Marine Research, 33(3), 325-340.

- Wooster, W.S. and J.H. Jones (1970) California Undercurrent Off Baja California. Journal of Marine Research, 28(2), 235-250.

- Wyllie, J.G. (1966) Geostrophic flow of the California Current at the surface and 200m. California Cooperative Oceanic Fisheries Investigations Atlas #4, XIII ppand 288 charts.

INITIAL DISTRIBUTION LIST